

# Distributed Control of Charging for Electric Vehicle Fleets Under Dynamic Transformer Ratings

Micah Botkin-Levy, Alexander Engelmann, *Member, IEEE*, Tillmann Mühlpfordt<sup>1</sup>, *Member, IEEE*,  
Timm Faulwasser<sup>2</sup>, *Member, IEEE*, and Mads R. Almassalkhi<sup>3</sup>, *Senior Member, IEEE*

**Abstract**—Due to their large power draws and increasing adoption rates, electric vehicles (EVs) will become a significant challenge for electric distribution grids. However, with proper charging control strategies, the challenge can be mitigated without the need for expensive grid reinforcements. This article presents and analyzes new distributed charging control methods to coordinate EV charging under nonlinear transformer temperature ratings. Specifically, we assess the tradeoffs between required data communications, computational efficiency, and optimality guarantees for different control strategies based on a convex relaxation of the underlying nonlinear transformer temperature dynamics. Classical distributed control methods, such as those based on dual decomposition and alternating direction method of multipliers (ADMM), are compared against the new augmented Lagrangian-based alternating direction inexact Newton (ALADIN) method and a novel low-information, look-ahead version of packetized energy management (PEM). These algorithms are implemented and analyzed for two case studies on residential and commercial EV fleets with fixed and variable populations. The latter motivates a novel EV hub charging model that captures arrivals and departures. Simulation results validate the new methods and provide insights into key tradeoffs.

**Index Terms**—Alternating direction method of multipliers (ADMM), augmented Lagrangian-based alternating direction inexact Newton (ALADIN), distributed optimization, dual decomposition, electric vehicle (EV) charging, fleet, packet-based coordination.

## I. INTRODUCTION

**A**S RENEWABLE generation is increasingly deployed, powering our transportation system from the electric

Manuscript received June 24, 2021; accepted September 20, 2021. Manuscript received in final form October 13, 2021. This work was supported in part by the U.S. Department of Energy’s Advanced Research Projects Agency–Energy (ARPA-E) under Award DE-AR0000694. Recommended by Associate Editor C. Manzie. (*Corresponding author: Mads R. Almassalkhi.*)

Micah Botkin-Levy is with NextEra Energy Resources, Juno Beach, FL 33408 USA (e-mail: micahkaye@gmail.com).

Alexander Engelmann and Timm Faulwasser were with the Institute for Automation and Applied Informatics, Karlsruhe Institute of Technology, 76131 Karlsruhe, Germany. They are now with the Department of Electrical Engineering and Information Technology, Institute for Energy Systems, Energy Efficiency and Energy Economics, TU Dortmund University, 44227 Dortmund, Germany (e-mail: alexander.engelmann@tu-dortmund.de; timm.faulwasser@ieee.org).

Tillmann Mühlpfordt is with DB Systel GmbH, 60326 Frankfurt, Germany (e-mail: tillmann.muehlpfordt@kit.edu).

Mads R. Almassalkhi is with the Department of Electrical and Biomedical Engineering, The University of Vermont, Burlington, VT 05405 USA, and also with Packetized Energy, Burlington, VT 05405 USA (e-mail: malmassa@uvm.edu).

Color versions of one or more figures in this article are available at <https://doi.org/10.1109/TCST.2021.3120494>.

Digital Object Identifier 10.1109/TCST.2021.3120494

grid, instead of fossil fuels, will reduce emissions and climate change impacts. In addition, falling lithium-ion battery prices [1] and low maintenance costs [2] will further increase adoption rates for both residential and commercial electric vehicles (EVs). However, there are certain challenges associated with the increased adoption of EVs. Specifically, uncoordinated charging from EVs can lead to demand that exceeds the rating of the distribution substation power transformer [3]. The MVA-scale transformers have cores that are immersed in mineral oil for improved heat transfer. However, EVs will increase the loading on a transformer and result in a higher hot-spot temperature, which is the transformer’s highest internal temperature. The hot-spot temperature is a major factor in transformer wear-and-tear and aging as the hot oil will break down the winding insulation faster [4]. To accurately model the transformer hot-spot temperature dynamics, a high-order, nonlinear thermodynamic model, such as the IEEE Standard C57.91-1995 (e.g., Clause 7 and Annex G), is often used [5]. However, low-order predictive transformer models (similar to those used herein) have been a topic of research for many years, including accurate regression-based [6], [7] and machine learning [8], [9] models for online estimation and operation and piecewise linear (PWL) approximations [10] for planning purposes. Some of these models are also capable of adapting to different forced air/direction oil operating modes.

Thus, it is desirable to manage the charging rate of EVs with respect to the transformer’s hot-spot temperature limit and EV-specific objectives and constraints, which can be formulated as a multiperiod scheduling problem. Due to a potentially large number of EVs and a long (overnight) prediction horizon, this scheduling problem can be computationally intensive and require full-state information, which can raise data privacy concerns. Techniques, such as primal or dual decomposition, are helpful in decoupling a large scheduling problem with coupling constraints into many smaller problems. Two classical algorithms for this purpose are dual decomposition and alternating direction method of multipliers (ADMM). In this article, we present two novel distributed methods and compare them against the two classical methods in terms of how effectively they converge to a solution (i.e., processing), the required data communications (i.e., privacy), and optimality of the solution (i.e., performance).

For a general comparison of noncentralized control techniques in electric power systems, please see the survey

in [11].<sup>1</sup> There are numerous papers that utilize dual decomposition [15], [16] and the ADMM approaches [17]–[21] to solve various EV charging (EVC) problem formulations. Other works employ novel and creative approaches, such as [23] and [24], which coordinate EVC under static transformer and voltage constraints using dual decomposition with reactive power compensation [22] and a shrunken-primal-dual subgradient algorithm that achieves valley-filling (grid-centric) objectives [23]. Zhou *et al.* [25], Ma *et al.* [26], and Gan *et al.* [27] leveraged game theory for large populations of EVs, where the average charging dynamics can be steered to a globally optimal solution with fast convergence on the order of 1–100 iterations depending on system parameters.

The above works focus on specific information scenarios, such as full information, shared (neighbors), or decentralized (nonshared) information. However, with increased interest in controlling EVC comes a growing concern for protecting EV owners' information. This can be achieved by reducing the need to communicate information to a central coordinator and, instead, use peer-to-peer technologies to enable transactive energy trading [27], [28].

In this article, we compare the privacy offered by the classical algorithms of dual ascent and ADMM and new EVC algorithms, i.e., the augmented Lagrangian-based alternating direction inexact Newton (ALADIN) method [29] and the packetized energy management (PEM) [30]–[33]. This comparison is based on protecting valuable customer information, such as personal travel schedules. To the best of the authors' knowledge, there is limited work that develops and compares noncentralized EVC algorithms subject to dynamic capacity constraints. For example, Ma *et al.* [21] computed the optimal scheduling of EVs under static capacity constraints and compares the tradeoff between the convergence speed and the amount of communication required. However, the study only considers different combinations of two similar algorithms and neglects the transformer temperature dynamics.

Furthermore, while much of the literature focuses on residential EVC, fewer papers consider charging needs of fleets or hubs of commercial EVs, such as school buses or delivery trucks, which engender different charging models. One paper aggregates EVs and optimizes the lowest electricity charging cost solution under linearized power flow constraints [34]. Another studies time-of-use pricing for a parking garage of EVs [35]. Other works coordinate aggregated EVs for use as a virtual battery [36], [37] or for frequency control [38] without considering individual EVs or local grid constraints. Here, we develop a new energy-based fleet charging model that incorporates charging requirements of the individual EVs.

With this work, we build on the initial model predictive control (MPC) approach from [39] but employ and analyze a convex relaxation of a practical nonlinear model for the

transformer temperature dynamics and augment analysis with two novel, distributed EVC schemes. While most previous works on predictive EVC control focus on one method for a specific setting, this article also compares multiple distributed methods and studies the tradeoffs between information sharing, performance, and computational processing requirements. Specifically, this article leverages a new distributed optimization method with quadratic convergence, i.e., ALADIN [29], and it also proposes the new iteration-free, packet-based coordination scheme [30]–[33]. These different methods have hitherto not been developed or analyzed for the EVC problem under dynamic coupling constraints. Note that prior work on PEM for EVs only considered static charging constraints and defined device priorities based on the charging constraint rather than the device's local energy state [30]. Thus, to incorporate the dynamic constraints within PEM, we first extend the device-driven, locally defined, energy-based load prioritization scheme to incorporate EVs' desired states of charge (SoCs) and departure times [31]–[33]. Specifically, we extend the approach in [31]–[33] with a novel look-ahead, mixed-integer quadratically constrained quadratic program (MIQCQP) to account for the temperature dynamics and packet requests. Furthermore, we present a novel modeling framework for an EVC hub that specifically enables the synchronous distributed EVC algorithms to apply to fleets of EVs with known, but time-varying arrivals and departures. Finally, we compare the role of information across different EVC methods via two highly relevant case studies. While the EVC problem is technically challenging, it is also of immediate practical relevance for EV fleet operators [40] and distribution grid operators [3], as it represents the equivalent of a cheap, universal software-based upgrade to any transformer.

In Section II, we formulate the nonlinear, thermal transformer model and local EV user energy/power constraints, and in Section III, we present a convex reformulation, which is rigorously analyzed. Then, in Section IV, we develop two new, noncentralized EVC algorithms, namely ALADIN and PEM, and briefly discuss the practical considerations facing a utility or a third-party coordinator/aggregator. We present two case studies in Sections V and VI to validate our methods against conventional methods from the literature, model time-varying arrivals and departures, and to serve as a comparison in Section VII. We conclude this article with a summary of this article and recommendations for future research directions in Section VIII.

## II. PROBLEM FORMULATION

Consider a finite collection of  $N$  EVs with charging stations that are served by the same balanced distribution-level substation transformer. Between a charger in the secondary network and the substation transformer in the primary network is a pole-top transformer, as shown in Fig. 1. A dynamic transformer temperature model is used in the EVC formulation to keep the substation transformer hot-spot temperature below its limits while satisfying the local EV user constraints. The goal is to regulate the charging of all EVs within the transformer temperature limit. This gives rise to an MPC problem that is

<sup>1</sup>We remark that the notions of distributed and decentralized computation are not unified in the literature. Here, we use the terminology from the optimization community [12], [13], where distributed computation allows a small amount of central coordination activity and decentralized computation avoids central coordination and relies on neighbor-to-neighbor communication only. We remark that in the control systems context, decentralized algorithms do not allow for any communication exchange [11], [14], while algorithms comprising a coordinator are denoted as hierarchical.

TABLE I  
EV AND TRANSFORMER NOMENCLATURE

Variable	Description	Domain	Units
<i>System-wide parameters</i>			
$N$	Number of EVs	$\mathbb{Z}_+$	-
$T_a(k)$	Ambient temperature at time $k$	$\mathbb{R}_+$	$^\circ\text{C}$
$i_d(k)$	Secondary background current at time $k$	$\mathbb{R}_+$	kA
$R$	Primary-secondary voltage ratio	$(0,1]$	-
$T^{\max}$	Transformer temperature limit	$\mathbb{R}_+$	$^\circ\text{C}$
$\gamma$	Ohmic losses-to-temp	$\mathbb{R}_+$	$^\circ\text{C}/\text{A}^2$
$\tau$	Temp time constant	$\mathbb{R}_+$	-
$\rho$	Ambient-to-temp losses	$\mathbb{R}_+$	-
$K$	Optimization horizon length	$\mathbb{Z}_{++}$	# of time steps
$\Delta t$	Time step length	$\mathbb{R}_{++}$	Seconds
<i>EV-specific parameters for EV <math>n</math></i>			
$i_n^{\max}$	Current limit	$\mathbb{R}_+$	A
$\alpha_n$	Charging efficiency	$[0,1]$	-
$\beta_n$	Battery capacity	$\mathbb{R}_+$	J
$\eta_n$	Normalized battery size	$\mathbb{R}_+$	$1/\text{A}$
$\bar{s}_n$	Minimum required SoC	$[0,1]$	-
$\bar{k}_n$	Latest time step to reach $\bar{s}_n$	$[0,K]$	-
$q_n, r_n$	Penalties on partial SoC, current draw	$\mathbb{R}_+$	-

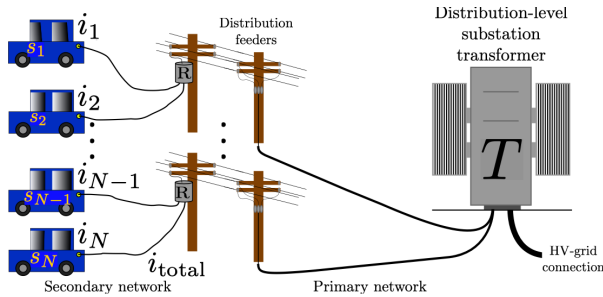


Fig. 1. Cartoon of the residential system setup, where the substation transformer's low-voltage (LV) side is in the primary network ( $V_{\text{pri}} = 8320$  V), while the chargers reside in the secondary network ( $V_{\text{sec}} = 240$  V).

described at each time instance by the following finite-horizon optimal control problem (OCP):

$$\begin{aligned}
 \min_{\mathbf{u}(0), \dots, \mathbf{u}(K-1)} & \sum_{n=1}^N \sum_{k=0}^{K-1} q_n (x_n(k) - x_n^{\text{ref}}(k))^2 + r_n (u_n(k))^2 \\
 \text{s.t.} & \mathbf{f}_k(\mathbf{x}(k+1), \mathbf{x}(k), \mathbf{u}(k)) = \mathbf{0} \\
 & \mathbf{h}_k(\mathbf{x}(k), \mathbf{u}(k)) \leq \mathbf{0} \\
 & x_n(k) \in \mathcal{X}_{n,k}, \quad u_n(k) \in \mathcal{U}_{n,k}, \quad x_n(0) = x_{\text{meas},n}
 \end{aligned}$$

for  $k = 0, \dots, K-1$  and  $n = 1, \dots, N+1$ , where  $\mathbf{x}(k) \doteq [x_1(k), \dots, x_N(k), x_{N+1}(k)]^\top \in \mathbb{R}^{N+1}$  represents the  $N$  SoCs for the EVs plus the one transformer temperature state each over the  $K$  time steps in the prediction horizon.<sup>2</sup> The control inputs  $\mathbf{u}(k) \doteq [u_1(k), \dots, u_N(k)]^\top \in \mathbb{R}^N$  include the EVC rates. Functions  $\mathbf{f}_k$  and  $\mathbf{h}_k$  account for inequality and equality constraints at time  $k$ , respectively, and are described in Sections II-A–II-E along with the objective function. The objective function's parameters  $q_n \geq 0, r_n > 0$  represent the EV owner's preference for achieving the state reference value with minimal control effort. The compact,

<sup>2</sup>In this work, the control and prediction horizons are assumed identical as the focus herein is on developing and comparing different novel algorithms.

convex sets  $\mathcal{X}_{n,k}, \mathcal{U}_{n,k}$  capture box constraints for states and inputs at time  $k$ . Table I lists parameters.

### A. Transformer Dynamics and Constraints

We consider a nonlinear hot-spot temperature model similar to that developed and validated in [6] and [9]

$$\dot{T}(t) = aL(t)^2 - b[T(t) - \tilde{T}_a(t)] + \tilde{c} \quad (1)$$

where  $T(t)$  represents the hot-spot temperature,  $L(t)$  is the apparent power demand [volt-ampere (VA)], and  $\tilde{T}_a(t)$  is the ambient temperature at time  $t \in \mathbb{R}_+$ . The constant coefficients  $a, b$ , and  $\tilde{c}$  represent the combined effects of conduction, convection, and radiation associated with transformer loading and ambient temperature, respectively. These parameters may be estimated from experimental data (as done in [6] and [9]) or from manufacturer spec sheets for a single, fixed air/oil operating mode (e.g., oil natural air natural/forced or ONAN/ONAF). In this article, the parameters are scaled versions of those in [9] such that the resulting model matches the timescale of the temperature responses given in spec sheets for the MVA-scale transformers used herein.

Using a zero-order hold with time step  $\Delta t$  for the inputs and exact discretization, the discrete-time dynamics are

$$T(k+1) = \tau T(k) + \tilde{\gamma} (L(k))^2 + \rho (\tilde{T}_a(k) + c) \quad (2)$$

for measured initial temperature of  $T(0) = T_{\text{meas}}$ , where  $\tau = e^{-b\Delta t}$ ,  $\rho = 1 - \tau$ ,  $c = (\tilde{c}/b)$ , and  $\tilde{\gamma} = (\rho/b)a$ .

Since the control variables of interest are the EVC currents, we will use a current-based model instead of a power-based model.<sup>3</sup> Thus, we decompose  $L(k) \doteq i_{\text{total}}^{\text{pri}}(k)V_{\text{pri}}$ , where  $i_{\text{total}}^{\text{pri}}(k)$  is the total Rms current magnitude from the primary network side of the transformer at time  $k$  and supplied at fixed, rated rms voltage  $V_{\text{pri}}$ . Since the EV charger is supplied from the secondary network, its rms voltage rating is  $V_{\text{sec}} \doteq RV_{\text{pri}}$ , where  $R \in (0, 1]$  is the pole-top transformer's fixed voltage ratio. The current  $i_{\text{total}}^{\text{pri}}(k)$  is based on the total primary-side equivalent transformer load from the secondary network, i.e.,  $i_{\text{total}}^{\text{pri}}(k) = Ri_{\text{total}}(k)$ , where  $i_{\text{total}}(k)$  is composed of the background demand,  $i_d(k)$ , and all EVC currents,  $i_n(k)$ , in the secondary network and

$$i_{\text{total}}(k) = i_d(k) + \sum_{n=1}^N i_n(k).$$

Thus, we can rewrite (2) in terms of  $i_{\text{total}}$  as

$$T(k+1) = \tau T(k) + \gamma (i_{\text{total}}(k))^2 + \rho (T_a(k)) \quad (3)$$

where  $\gamma = \tilde{\gamma} V_{\text{pri}}^2 R^2$  and  $T_a(k) \doteq \tilde{T}_a(k) + (\tilde{c}/b)$ . In addition, the temperature  $T(k)$  is constrained by the hot-spot temperature limit  $T^{\max}$ .

<sup>3</sup>Since the focus herein is on EV scheduling algorithms, the power system details associated with multiphase distribution feeders and transformers, voltage fluctuations, and power factors are not discussed.

### B. EV Dynamics and Constraints

The continuous-time, normalized charging dynamics of vehicle  $n$  with current  $i_n(t)$  are modeled as

$$\dot{s}_n(t) = \tilde{\eta}_n i_n(t), \quad s_n(t) \in [0, 1] \quad (4)$$

where  $\tilde{\eta}_n \doteq (\alpha_n/\beta_n)V_{\text{sec}}$  is the normalizing ratio of the vehicle's charging efficiency ( $\alpha_n$ ) to battery capacity ( $\beta_n$ ) and supplied secondary rms voltage,  $V_{\text{sec}}$ . The discrete-time equation is

$$s_n(k+1) = s_n(k) + \eta_n i_n(k), \quad s_n(0) = s_{\text{meas},n} \quad (5)$$

for measured initial SoC  $s_{\text{meas},n}$ . Each charger has a current,  $i_n(k) \in [0, i_n^{\text{max}}]$ .

### C. EV Owner Preferences

All residential vehicles are assumed to be available for charging at the beginning of the time period considered and owners have varying requirements for when they need their vehicle. The owners of the devices determine a minimum SoC ( $\bar{s}_n$ ) that must be met by a specific time step ( $\bar{k}_n$ ). The associated constraint for the  $n$ th vehicle is

$$s_n(k+1) \geq \hat{s}_n(k+1) \doteq \begin{cases} \bar{s}_n, & k+1 \geq \bar{k}_n \\ 0, & \text{else.} \end{cases} \quad (6)$$

In addition, the user can set their preference for the tradeoff between charging their EV quickly and minimizing local battery wear and control effort. This is achieved by selecting parameters in the objective function and is described next.

### D. EVC Control Objective

The  $n$ th EV owner's charging preference is used in the objective function to prioritize charging rate against the SoC as

$$J_n(\mathbf{i}_n, \mathbf{s}_n) \doteq \sum_{k=0}^{K-1} q_n (s_n(k+1) - 1)^2 + r_n (i_n(k))^2. \quad (7)$$

Specifically, for each vehicle  $n$ , we define  $M_n \doteq (q_n/r_n)\eta_n^2$  based on a user-defined ratio ( $q_n/r_n$ ) and fixed EV parameter  $\eta_n > 0$ . This ratio  $M_n$  will be used in Section II-E to provide sufficient conditions under which we can guarantee that a suitable convex relaxation is tight. These conditions are necessary due to the fundamental tradeoff in the objective function between reaching full charge quickly (large  $M_n$  to maximize SoC) and keeping the battery charge rate low (small  $M_n$  to minimize control effort), which serves as a proxy for wear and tear. This objective function is similar to a linear quadratic regulator (LQR) that penalizes deviations in SoC from unity and large control efforts. Summing over all  $N$  vehicles yields the total cost metric, which we seek to minimize in the optimization problem. Finally, note that vehicle-to-grid (V2G) technology is unavailable in this setup. However, from the transformer constraints defined in Section II-A and the objectives in (7), there is no value added with V2G.

*Remark (Valley Filling):* Note that one could augment the objective function with a linear term that depends on the difference between predicted transformer temperature and

the transformer temperature limit  $\sum_{k=1}^K \psi_k (T(k) - T^{\text{max}})$  with  $\psi_k \geq 0$ . The EV fleet operator would then be able to tune parameter  $\psi_k$  based on how valuable underloading is (i.e., spreading charging evenly over time). As  $\psi_k$  increases the formulation then shifts from a consumer-centric focus that allows early charging to a valley-filling, utility-centric approach, which optimizes charging based on the grid's availability. Valley filling a rich area of research that includes peer-to-peer, decentralized, and consensus-based methods of coordination, which is beyond the scope of this article [24], [25], [41].

### E. Centralized OCP

The open-loop OCP arises from the combination of the above constraints and objective function for all EVs and time steps. It reads

$$\min_{i_n(k)} \sum_{n=1}^N \sum_{k=0}^{K-1} q_n (s_n(k+1) - 1)^2 + r_n (i_n(k))^2 \quad (8a)$$

$$\text{s.t. } T(k+1) = \tau T(k) + \gamma (i_{\text{total}}(k))^2 + \rho T_a(k) \quad (8b)$$

$$s_n(k+1) = s_n(k) + \eta_n i_n(k) \quad (8c)$$

$$i_{\text{total}}(k) = i_d(k) + \sum_{n=1}^N i_n(k) \quad (8d)$$

$$T(k+1) \leq T^{\text{max}} \quad (8e)$$

$$s_n(k+1) \in [\hat{s}_n(k+1), 1] \quad (8f)$$

$$i_n(k) \in [0, i_n^{\text{max}}] \quad (8g)$$

$$T(0) = T_{\text{meas}}, \quad s_n(0) = s_{\text{meas},n} \quad (8h)$$

for all  $k = 0, \dots, K-1$  and  $n = 1, \dots, N$ . This is a nonconvex nonlinear program (NLP) due to the nonlinear (8b). Note that the only coupling constraint between the transformer and EV decisions is (8d). Previous work in [39] used a linearized temperature model to simplify the coupling. Finally, note that the formulation herein assumes ideal parameter values with no uncertainty.

## III. CONVEXIFICATION OF CENTRALIZED EVC PROBLEM

To overcome the nonconvexity of (8b), we consider two different relaxations: an epigraph relaxation, which yields a second-order cone program (SOCP), and a PWL relaxation. The former replaces the quadratic equality (8b) with the linear equality and quadratic inequality

$$T(k+1) = \tau T(k) + \gamma e(k) + \rho T_a(k) \quad (9)$$

$$e(k) \geq (i_{\text{total}}(k))^2. \quad (10)$$

Under this relaxation, problem (8) becomes an SOCP. The benefit of this approach is that if (8e) is strictly active at time  $k$ , then (10) is satisfied with equality for all prior time steps and we recover the nonlinear model exactly. This is guaranteed by the following theorem and corollary.

*Theorem 1 (Main Result):* Given fixed EV parameters  $r_n \geq 0$ ,  $\eta_n, q_n > 0$ . If, at optimality, there exists  $n, k$  for which

$i_n(k) < i_n^{\max}$  (i.e., an EV charger is throttled) and SoC satisfies

$$s_n(k+1) < \begin{cases} 1, & \text{if } r_n = 0 \\ \frac{M_n + s_n(0)}{M_n + 1}, & \text{if } r_n > 0 \end{cases}$$

then  $e(l) = (i_{\text{total}}(l))^2 \forall l \leq k$  in (10).

The proof is based on the Karush–Kuhn–Tucker (KKT) analysis and is provided in the Appendix. Note that when  $r_n > 0$ , Theorem 1 provides a method to choose  $q_n$  and  $r_n$  based on constant  $\eta_n$  and a desirable upper threshold on SoC. Ideally, one would choose a threshold of 1, but this requires  $r_n = 0$ , which may not be reasonable. Instead, one could solve for  $M_n$  by setting  $M_n/(M_n + 1) > \bar{s}_n$  [ignoring the initial state,  $s_n(0)$ ], which then neatly embeds the user-defined quality-of-service (QoS) constraint into the objective function parameters. For example, if  $\bar{s}_n = 0.8$ , one can choose  $M_n > 4$ , which implies  $q_n/r_n > (4/\eta_n^2)$ .

*Remark (Tightness of the SOCP Relaxation):* At optimality, it may not be the case that any EV  $n$  satisfies Theorem 1's conditions:  $i_n(k) < i_n^{\max}$  and  $s_n(k+1) < (M_n + s_n(0))/(M_n + 1)$  for some time step  $k$ , that is, the optimal solution may not be tight, if for all EVs  $n$  and for entire prediction horizon  $k$  either: 1)  $i_n(k) = i_n^{\max}$  or 2)  $s_n(k+1) \geq (M_n + s_n(0))/(M_n + 1)$ . In case I, EVs are all charging at their maximum charge rates and never throttled, which indicates underutilized capacity from the transformer. For case II, the tradeoffs from the objective function imply that any EVs that may be throttled must have a sufficiently high SoC and are not negatively impacted by the transformer's capacity. Together, cases I and II imply that (8e) may not be strictly active, so the temperature state in (9) and the convex relaxation (10) can be removed without affecting the optimal solution. Thus, outside of Theorem 1's conditions, the convex relaxation has no impact on the optimal solution, which ensures that no feasible solution for the relaxed SOCP formulation will lead to overheating of the transformer.

Finally, to relate the transformer's temperature state and safety limit (8e) to the tight convex relaxation above, we present the following corollary. Together with Theorem 1, this corollary guarantees that if the temperature limit (8e) is strictly active at time  $k+1$ , then the convex relaxation is tight for all prior time steps.

*Corollary 1 (Temperature Limit):* For the SOCP, at optimality,  $k+1$  is the last instance for which (8e) is strictly active, if and only if,  $k$  is the largest integer for which (10) is tight.

Despite the guarantee of tightness for the relaxed model at optimality, the quadratic constraints increase the complexity of complementary conditions and beget numerical difficulties. To overcome this challenge, a PWL approach is used to formulate the nonlinear problem as a quadratic program (QP), which improves the numerics of the problem significantly. An additional benefit of the PWL approximation is that the linear segments dominate the quadratic model and, thus, is designed to overestimate the transformer current, as shown in Fig. 2. This overestimate is a function of the number of segments and creates a conservative prediction of the transformer temperature when the underlying nonlinear model

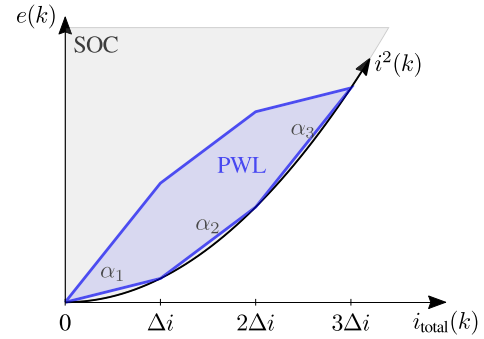


Fig. 2. Relaxing the nonconvexity  $e(k) = (i_{\text{total}})^2$  with a PWL approximation that does not enforce adjacency conditions (blue) and a conic relaxation (gray). Note that the PWL approximation assumes that  $I^{\max} = 3\Delta i$ .

is exact. Therefore, for the remainder of this article, we focus on the PWL implementation.

#### A. PWL Approximation

Define  $e(k)$  as a PWL approximation of  $i_{\text{total}}(k)^2$  with  $M$  segments of equal width  $\Delta i \doteq (I^{\max}/M)$  as shown in Fig. 2, where  $I^{\max}$  is an upper bound on transformer current. Then, we obtain

$$i_{\text{total}}(k)^2 \leq \text{PWL}\{i_{\text{total}}(k)^2\} =: e(k) = \sum_{m=1}^M \alpha_m i_m^{\text{PW}}(k) \quad (11)$$

where  $i_m^{\text{PW}}(k) \in [0, \Delta i]$  represent auxiliary PWL variables for each segment  $m$  a time  $k$  such that  $\sum_{m=1}^M i_m^{\text{PW}}(k) \doteq i_{\text{total}}(k)$  and slope parameters  $\alpha_m \doteq (2m-1)\Delta i$ .

Note that this PWL approximation relaxes the adjacency conditions<sup>4</sup> that are usually enforced for the PWL segments, which avoids a mixed-integer formulation and creates the blue convex relaxation shown in Fig. 2. Using this directly in the transformer constraint relaxes the NLP to a QP

$$T(k+1) = \tau T(k) + \gamma \left( \Delta i \sum_{m=1}^M (2m-1) i_m^{\text{PW}}(k) \right) + \rho T_a(k). \quad (12)$$

*Remark (Upper Bound on PWL Error):* Since we are using equal width segments, the maximum error between the PWL approximation and the actual  $i^2$  is just the maximum distance between the linear segment (PWL( $i$ )) and the quadratic curve ( $q(i)$ ) at the midpoint [i.e.,  $(\Delta i/2) \doteq (I^{\max}/2M)$ ]

$$\begin{aligned} \epsilon_i^{\max} &= \text{PWL}\left(\frac{\Delta i}{2}\right) - q\left(\frac{\Delta i}{2}\right) = \frac{(I^{\max})^2}{2M^2} - \left(\frac{I^{\max}}{2M}\right)^2 \quad (13) \\ &\Rightarrow \epsilon_i^{\max} = (I^{\max})^2 (4M^2)^{-1}. \quad (14) \end{aligned}$$

Multiplying by  $\gamma$  provides the upper bound on the corresponding temperature error

$$\epsilon_T^{\max} = \gamma (I^{\max})^2 (4M^2)^{-1}. \quad (15)$$

Even for a large current  $I^{\max} = 0.72$  kA with  $\gamma = 15.74^\circ\text{C}/(\text{kA})^2$  and  $M = 6$  segments, the maximum error

<sup>4</sup>Adjacency conditions enforce  $i_m^{\text{PW}}(k) > 0 \Rightarrow i_p^{\text{PW}}(k) = \Delta i \forall p < m$ .

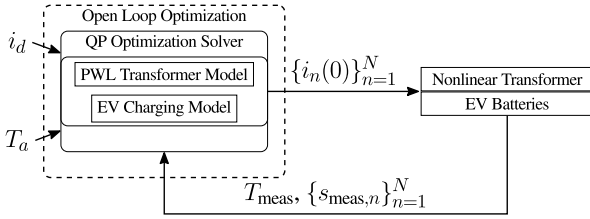


Fig. 3. OCP with feedback. The OCP is used with the ALADIN, ADMM, and dual decomposition methods and employs the PWL approximation of the transformer’s nonlinear current–temperature relations in the OCP formulation, while the plant model represents the nonlinear transformer.

between a PWL’s linear prediction of the transformer temperature ( $T_{PWL}$ ) and the quadratic temperature ( $T_q$ ) for a single time step is  $\epsilon_T^{\max} \doteq T_{PWL}(k+1) - T_q(k+1) = 0.057^\circ\text{C}$  when the convex relaxation is tight. While this temperature error accumulates over time steps in the open-loop prediction, it is also discounted over time since  $\tau < 1$ . Therefore, the PWL approximation provides a feasible and robust estimate of the nonlinear temperature dynamics.

### B. Centralized PWL Problem

The PWL relaxation provides an approximation of the transformer dynamics in (12) and replaces (8b). In addition, the coupling constraint between the transformer’s (PWL) current segments and the EVC currents is now

$$i_d(k) + \sum_{n=1}^N i_n(k) = \sum_{m=1}^M i_m^{\text{PW}}(k) \doteq i_{\text{total}}(k). \quad (16)$$

Also, we enforce limits on the variable associated with each linear segment

$$i_m^{\text{PW}}(k) \in [0, \Delta i]. \quad (17)$$

The PWL formulation adds one more set of box constraint than the NLP formulation and replaces the optimization variables  $\mathbf{i}_{\text{total}} \in \mathbb{R}^K$  with  $\mathbf{i}^{\text{PW}} \in \mathbb{R}^{MK}$ . This open-loop OCP is then implemented in receding-horizon fashion, as shown in Fig. 3.

*Remark (Extending Theorem 1 to the PWL Formulation):* Since the PWL relaxation overestimates the nonconvex equality constraint, it is contained within the SOCP relaxation (as in Fig. 2). This ensures, under the same conditions of Theorem 1 and Corollary 1, that the optimal solution from the PWL formulation is tight relative to the PWL segments. Thus, the PWL formulation can successfully predict and regulate the transformer’s dynamic temperature trajectory relative to its temperature limit. For a detailed treatment of the PWL relaxation, please see [42].

## IV. NONCENTRALIZED IMPLEMENTATION

The centralized problem can be decomposed into  $N$  sub-problems if it were not for the coupling constraints (16). Thus, in this section, we present different distributed and decentralized charging algorithms. Specifically, ALADIN and PEM represent two novel contributions for EVC control, while the other two methods (dual ascent and ADMM) serve as base cases for comparison.

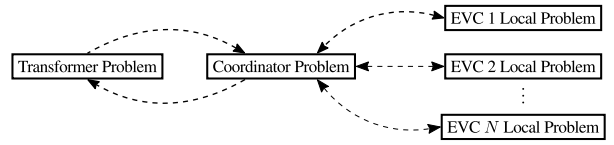


Fig. 4. Distributed EVC coordination scheme. Synchronous schemes require the communications from all  $N + 1$  local problems before solving with the coordinator problem.

The iterative ALADIN, dual ascent, and ADMM schemes employ the partial Lagrangian with respect to (16) as follows:

$$\begin{aligned} \mathcal{L}(\mathbf{i}_n, \mathbf{s}_n, \mathbf{i}_m^{\text{PW}}, \lambda) &= \sum_{n=1}^N J_n(\mathbf{i}_n, \mathbf{s}_n) + \lambda^\top \left( \mathbf{i}_d + \sum_{n=1}^N \mathbf{i}_n - \sum_{m=1}^M \mathbf{i}_m^{\text{PW}} \right) \\ &= \sum_{n=1}^N (J_n(\mathbf{i}_n, \mathbf{s}_n) + \lambda^\top \mathbf{i}_n) + \lambda^\top \left( \mathbf{i}_d - \sum_{m=1}^M \mathbf{i}_m^{\text{PW}} \right) \end{aligned} \quad (18)$$

where  $\lambda \in \mathbb{R}^K$  are the Lagrange multipliers associated with (16). From (18), the Lagrangian can be separated into local EV variables  $\{\mathbf{i}_n, \mathbf{s}_n\} \in \mathbb{R}^{2NK}$  and transformer variables  $\{\mathbf{i}^{\text{PW}}\} \in \mathbb{R}^{MK}$ , which turns (18) into a separable objective function subject to decoupled constraints. This means that the optimization problem can be solved in a distributed fashion by iteratively updating  $\lambda$  for which we develop and present dual ascent, ADMM, and ALADIN algorithms. We also provide a noniterative packet-based coordination scheme adapted from PEM. Each algorithm has different requirements for the transformer, EVs, and coordinator problems, as shown in Fig. 4. Next, we will discuss each scheme, and since dual decomposition and ADMM are two common methods, details have been omitted in this article.

### A. ALADIN

ALADIN is a relatively new distributed optimization algorithm [29]. It has been considered, among other things, for optimal power flow (OPF) problems [43]. The method decomposes the centralized optimization problem by having each agent solving its local problem based on the primal iterate guess of primal variables and the Lagrange multipliers of the coupling constraints. The local solutions together with first- and second-order information are provided to the coordinator to update the primal variables and multipliers by solving a centralized (but simple) QP to foster consensus. This setup allows predictive ALADIN to achieve quadratic convergence locally, which greatly reduces the number of iterations needed and is highly desirable.

The first two steps of ALADIN are shown in Algorithm 1 and solve local optimization problems for: 1) the EVs and 2) the transformer. Here, the primal variables for the EVs are collected in  $\mathbf{x}_n^\top = ((\mathbf{i}_n)^\top, (\mathbf{s}_n)^\top)$  and the primal variables for the transformer in  $\Delta \mathbf{x}_{N+1}^\top = ((\mathbf{i}_{N+1})^\top, (\mathbf{T})^\top)$  with  $(\mathbf{i}_{N+1})^\top = (\mathbf{i}_1^{\text{PW}\top}, \dots, \mathbf{i}_M^{\text{PW}\top})^\top$ , where the latter is due to the PWL formulation (11). As mentioned, the primal solution from each local EV and transformer problem is shared with the coordinator. In addition, the gradient and Hessian of

**Algorithm 1** ALADIN for EV Charging

**Initialization:** Initial ( $p \equiv 0$ ) guess of dual multiplier  $\lambda^{(0)}$ , of all four auxiliary variables  $\{\mathbf{i}_n^{(0)}, \mathbf{s}_n^{(0)}, \mathbf{i}_{N+1}^{PW(0)}, \mathbf{T}^{(0)}\}$  and tuning parameters  $\{\rho_{ALAD}, \mu, \sigma_z, \sigma_t, \{\sigma_{i,n}, \sigma_{s,n}\}_{n \in 1, \dots, N}\}$ .

**Repeat for  $p$ :**

1) *Solve local EV problems:* for each  $n \in 1, \dots, N$

$$\begin{aligned} \bar{\mathbf{i}}_n^{(p)} &= \arg \min_{\mathbf{i}_n, \mathbf{s}_n} J_n(\mathbf{i}_n, \mathbf{s}_n) + (\lambda^{(p)})^\top \mathbf{i}_n + \\ &\quad \frac{\rho_{ALAD} \sigma_{i,n}}{2} (\mathbf{i}_n - \mathbf{i}_n^{(p)})^2 + \frac{\rho_{ALAD} \sigma_{s,n}}{2} (\mathbf{s}_n - \mathbf{s}_n^{(p)})^2 \\ &\text{s.t. (8c), (8f), (8g)} \end{aligned}$$

2) *Solve local transformer problem:*

$$\begin{aligned} (\bar{\mathbf{i}}_{N+1})^{(p)} &= \arg \min_{\mathbf{i}_{N+1}, \mathbf{T}} -(\lambda^{(p)})^\top \sum_{m=1}^M \mathbf{i}_m^{PW} + \\ &\quad \frac{\rho_{ALAD} \sigma_z}{2} (\mathbf{i}_{N+1} - \mathbf{i}_{N+1}^{(p)})^2 + \frac{\rho_{ALAD} \sigma_t}{2} (\mathbf{T} - \mathbf{T}^{(p)})^2 \\ &\text{s.t. (12), (17), (8e)} \end{aligned}$$

3) *Solve coordinator problem:*

$$\begin{aligned} \min_{\Delta \mathbf{x}_n, y} \sum_{n=1}^{N+1} \left( \frac{1}{2} \Delta \mathbf{x}_n H_{x_n}^{(p)} \Delta \mathbf{x}_n + g_{x_n}^{(p)} \Delta \mathbf{x}_n \right) + (\lambda^{(p)})^\top y + \frac{\mu}{2} \|y\|^2 \\ \text{s.t. } \sum_{n=1}^N (\bar{\mathbf{i}}_n^{(p)}(k) + \Delta \bar{\mathbf{i}}_n(k)) - \sum_{m=1}^M (\bar{\mathbf{i}}_m^{PW}{}^{(p)}(k) + \Delta \bar{\mathbf{i}}_m^{PW}{}^{(p)}(k)) = \\ y(k) - i_d(k) \quad |\lambda_{QP}(k)| \\ \Delta T(k+1) = \tau \Delta T(k) + \gamma \left( \Delta i \sum_{m=1}^M (2m-1) \Delta \bar{\mathbf{i}}_m^{PW}{}^{(p)}(k) \right) \\ \Delta s_n(k+1) = \Delta s_n(k) + \eta_n \Delta i_n(k) \text{ for all } k=0, \dots, K-1 \\ C_{\bar{x}_n}^{(p)} \Delta \mathbf{x}_n \leq 0 \text{ for all } n=1, \dots, N+1 \end{aligned}$$

4) *Termination Criterion:* If

$$\begin{aligned} \left\| \bar{\mathbf{i}}_d(k) + \sum_{n=1}^N \bar{\mathbf{i}}_n(k)^{(p)} - \sum_{m=1}^M (\bar{\mathbf{i}}_m^{PW}{}^{(p)}(k)) \right\|_1 \leq \epsilon_1 \\ \text{and } \left\| \sigma_{x_n} (\bar{\mathbf{x}}_n^{(p)} - \mathbf{x}_n^{(p)}) \right\|_1 \leq \epsilon_2 \end{aligned}$$

then exit with  $x^* = x^{(p)}$  and  $i_n^*(0)$  is implemented in EVs.

5) *Update dual variable and auxiliary variables*

$$\begin{aligned} \mathbf{x}_n^{(p+1)} &= \bar{\mathbf{x}}_n^{(p)} + \Delta \mathbf{x}_n, \quad n=1, \dots, N+1 \\ \lambda^{(p+1)} &= \lambda_{QP}, \quad p \rightarrow p+1. \end{aligned}$$

the Lagrangian relative to  $\mathbf{x}_n$  are denoted as  $g_{x_n}$  and  $H_{x_n}$ , respectively. Note that the gradients of the box constraints  $C_{\bar{x}_n}^{(p)}$  are constant and given by zero vectors with  $-1$  or  $1$  in the column corresponding to a primal variable for which a box constraint is active. Thus, here, it suffices to communicate an index set of the active constraints instead of a full matrix. In Step 3, the coordinator combines the local information into a coordination QP to update the auxiliary variables and the dual variables. The specific ALADIN variant used for the EVC OCP is shown in Algorithm 1. A slight alteration to the ALADIN formulation is used, which changes the linearized expressions,  $C_{\bar{x}_n}^{(p)} \Delta \mathbf{x}_n$ , in Step 3 to be inequalities from their original equality constraints. This relaxation allows the local variables to move asymmetrically away from its bound instead of fixing all variables that are at their upper or lower limit.

ALADIN provides a systematic approach to decomposing our large centralized primal formulation into many small, local QPs, and a single coordination QP. However, despite the few iterations required for convergence (e.g., please see [29]), the information required from the subproblems is significant and the coordinator problem is computationally intensive. For a variant of ALADIN with reduced size of the coordination QP, we refer to [44]. Note that the ALADIN tuning parameters  $\rho_{ALAD}, \mu, \sigma_z, \sigma_t$  and  $\sigma_{i,n}, \sigma_{s,n} \forall n$  have to be chosen initially.

**B. Dual Decomposition**

Dual decomposition separates (18) and creates local QP EVC problems, a local LP transformer problem, and updates  $\lambda$  by dual ascent. Standard dual decomposition with dual ascent update for separable problems is used from [45] and the setup is similar to that of [39], except that here, we employ the relaxed PWL model and not a linearized model.

**C. ADMM**

ADMM builds on top of dual decomposition by augmenting the local objective functions using auxiliary variables. A separable ADMM approach is used here based on [46].

Note that both dual decomposition and ADMM can be expressed as a special case of ALADIN with considerably simplified coordination QP and, in case of dual decomposition, by choosing all  $\sigma_{(\cdot)}$ 's to zero additionally (cf. [29]). Also, these classical optimization methods are only used as bases for comparison in the case studies. For these reasons and since detailed treatments of these algorithms for EVC problems are widely available in the literature, we do not state them explicitly here.

**D. PEM With Dynamic Constraints**

PEM represents a computationally and informationally light demand-side coordinating scheme for coordinating distributed energy resources (DERs) (in real time), such as EV chargers. The scheme uses a stochastic, packet-based approach similar to modern communication networks to dynamically prioritize demand-side resources based on local energy needs [31]–[33]. The full PEM algorithm adapted for the EVC problem approximates the OCP and is described in Algorithm 2. Each local “packetized” charger can infer or measure its local energy need, which is mapped to a prescribed probability of requesting a fixed-duration ( $\delta > 0$ ) packet of energy (e.g., a  $\delta = 5$  step, constant-ampere charging epoch). The request is submitted to the coordinator, which considers real-time and/or predicted transformer conditions to either accept or reject the packet to maintain the transformer temperature within its limits. To ensure QoS for the device owner, opt-out logic enables EVs with immediate energy needs to temporarily exit the scheme and recover their SoC. Algorithm 2 is described next.

1) *Local EV Problem:* The PEM scheme does not require that the EVC agent solves a local optimization problem to manage EV charger demand. Instead, a “packetized” EV charger is assumed capable of accurately measuring the EV's

SoC,  $s_{\text{meas},n}$ , and inferring time until departure,  $\bar{k}_n$ . Based on these two updates, the EV charger calculates its energy need with the ratio

$$\text{ratio}_n(k) \doteq (\bar{s}_n - s_{\text{meas},n}(k))(\eta_n i_n^{\text{max}}(\bar{k}_n - k))^{-1} \in \mathbb{R}.$$

If the  $\text{ratio}_n > 1$ , then the time remaining is not sufficient to provide the desired energy, even if charging for the entire remaining duration. Thus, if  $\text{ratio}_n$  reaches or initially exceeds unity, then the device will automatically opt out (opt-out status denoted by  $\text{Req}_n < 0$ ) and continuously charge until the time of departure. Thus, opting out represents a background disturbance to the fleet of packetized EV chargers, which reduces the number of packets that can be accepted by the coordinator. When  $\text{ratio}_n \in [0, 1]$ , the value is mapped to a probability of requesting a packet over the duration of time step  $k$  (request status denoted by  $\text{Req}_n \in \{0, 1\}$ ), where a request from EV  $n$  is sent to the coordinator with exponential waiting times, e.g., please see Algorithm 2. The probability of requesting a packet depends on the ratio and a prespecified mean time-to-request (or mtrr) for a specific ratio value set point ( $\hat{r}_{\text{set},n} \in (0, 1)$ ). As  $\text{ratio}_n(k) \rightarrow 0/1$ , the probability of requesting a packet during time step  $k$  approaches 0/1. Of course, while the charger is “consuming” an energy packet, it does not request another packet, so  $\text{Req}_n(k)$  status is set to the negative of the packet completion timer.

If an EV requests a packet ( $\text{Req}_n \equiv 1$ ) and is notified that its packet is accepted, the EV charges at a prespecified current for  $\delta$  time steps. If  $\text{ratio}_n < 0$ , we denote status by  $\text{Req}_n \equiv 2$ , which implies that the EV’s SoC exceeds its desired (minimum) energy target, which means that the EV’s local “energy need” has been satisfied and any future requests from this EV are designated a low-priority request.

2) *Coordinator Problem*: The coordinator receives packet requests and must now accept a proportion of them in such a way as to keep the transformer temperature within limits. Since temperature is a dynamic state and prior work with PEM and EVs focused on static power or current limits, one major contribution of this article is the extension of PEM for scheduling under dynamic state constraints. Thus, this section extends prior work on PEM with a novel, predictive, synchronous coordinator formulation that utilizes an efficient MIQCQP formulation to select which requests are accepted and denied. Note that the predictive model in the coordinator only concerns the transformer temperature relative to changes in demand and does not extend to the fleet’s requests or SoC, that is, the coordinator uses a persistent forecast of requests and opt-outs over its prediction horizon, which is just  $\delta$  time steps (e.g.,  $\delta = 2$  time steps, which is 6 min in Case Study 1).

To do so, first, define the set of all devices that do not request a packet ( $\text{Req}_n(k) \equiv 0$ ) during time step  $k$  as  $\mathcal{E}_0$ . The EVs that request a packet at time  $k$  belong to set  $\mathcal{E}_1$ . Then, define  $\delta$  sets for the devices that are “locked in” for future time steps as  $\mathcal{Y}_l, l \in k + 1, \dots, k + \delta$  to capture the groups of EVs still consuming an energy packet or those that opted out earlier. Finally, define  $\mathcal{E}_2$  as the set of EVs that have already reached their desired (minimum) SoC target but are not fully charged.

The coordinator’s MIQCQP problem is solved in Algorithm 2 to determine which EVs have their packet requests accepted ( $\text{Resp}_n(k) = 1$ ) and rejected ( $\text{Resp}_n(k) = 0$ ). Since the problem looks ahead just a packet length, the prediction horizon is short and the formulation is efficient. The requests from  $\mathcal{E}_2$  are deprioritized by use of a scaling factor ( $\omega_E \doteq \min\{1/(NK), 1/(4N)\} \ll 1$ ) in the objective function. To ensure a solution always exists, a slack variable is added to the temperature limit and penalized in the objective function ( $\omega_S \gg 1$ ).

Finally, the MIQCQP depends on the EV chargers’ ampacities,  $i_n^{\text{max}}$ . The current rating is known exactly when the information is included in the request or may be approximated via data-driven methods. In this work, we assume the former. After solving the MIQCQP, the optimal solution,  $\mathbf{u}_{\text{ch}}^*(0) \in \mathbb{R}^N$ , represents the EV chargers whose requests were accepted by the coordinator. To reduce the necessary communications in an online implementation of PEM, only EVs whose charger’s logic state undergoes a transition [e.g.,  $\text{Resp}_n(k) \neq \text{Resp}_n(k - 1)$ ] are updated by the coordinator.

Sections V and VI explore the convex transformer temperature models and EVC algorithms within two different, but relevant scenarios: residential and commercial fleets of EVs. The latter will require novel modeling of a hub of commercial EVs that arrive and depart asynchronously. We then adapt the algorithms to manage the charging of multiple hubs rather than individual EVs. Finally, Section VII provides discussion and comparison between distributed methods employed in Case Studies 1 and 2.

## V. CASE STUDY 1: RESIDENTIAL PEV CHARGING

Now that we have developed several distributed control methods for the EVC problem, we consider a scenario and evaluate each method on privacy, performance, and processing metrics. Specifically, we consider a residential scenario with 100 EVs, for the overnight hours of 8 P.M. to 10 A.M. However, a similar setup could be relevant for large public or social events, such as overnight music festivals and sporting events (e.g., a 3-h sports event in a stadium), where many EVs park for an extended, co-incident period of time. The rest of the parameters used are shown in Table II where the bracket notation  $[a, b]$ , denotes the parameter’s range. For the look-ahead PEM, we use  $\delta = 2$  time steps,  $\text{mtrr} = \Delta t \delta = 2$  time steps (i.e.,  $2 \times 180 = 360$  s), and  $\hat{r}_{\text{set},n} = 0.10$ .

### A. Simulation Results

The OCP is solved in closed-loop to engender a receding-horizon simulation for each noncentralized algorithm, and the centralized formulation is shown in Fig. 5. The top two plots show the transformer temperature and total primary network load at the transformer. The bottom plot displays the dual multiplier  $\lambda$ , which is associated with the coupling constraint (16). In addition to the centralized OCP solution and the solutions from the four noncentralized algorithms, the result of the uncoordinated EVC is also provided. Clearly, without EVC control implemented, the transformer temperature exceeds its limit for hours.

**Algorithm 2** Look-Ahead PEM Algorithm

**Local EV Problem:** compute for each  $n \in N$

**if** Consuming Packet **then**

$\text{Req}_n(k) = -$  duration remaining for packet

**else if**  $s_{\text{meas},n}(k) = 1$  **then** ▷ EV at 100%

$\text{Req}_n(k) = 0$

**else if**  $s_{\text{meas},n}(k) \geq \bar{s}_n$  **then** ▷ EV is low priority

$\text{Req}_n(k) = 2$

**else**

$\text{ratio}_n(k) = (\bar{s}_n - s_{\text{meas},n}(k))(\eta_n i_n^{\text{max}}(\bar{k}_n - t))^{-1}$

**if**  $\text{ratio}_n(k) \geq 1$  **then**

$\text{Req}_n(k) = -\delta$  ▷ EV opts out

**else**

$\mu(k) = \frac{1}{mtr} \frac{\text{ratio}_n(k)}{1 - \text{ratio}_n(k)} \frac{1 - r_{\text{set},n}}{r_{\text{set},n}}$

$P_n(k) = \min\{\max\{1 - e^{-\mu(k)\Delta t}, 0\}, 1\}$

$\text{Req}_n(k) = \begin{cases} 1, & \text{rand}() < P_n(k) \\ 0, & \text{else} \end{cases}$

**End****Coordinator Problem:**

Update sets  $\mathcal{E}_0, \mathcal{E}_1, \mathcal{E}_2, \mathcal{Y}_k$  and measure  $T_{\text{meas}}$

Solve MIQCQP to determine  $\mathbf{u}_{\text{ch}}^*(k) \forall k \in \mathcal{K}_\delta \doteq \{0, \dots, \delta - 1\}$

$$\begin{aligned} & \max_{T_{\text{slack}}, u_n} \sum_{k=0}^{\delta-1} \left( \sum_{n \in \mathcal{E}_1} u_n(k) + \omega_E \sum_{n \in \mathcal{E}_2} u_n(k) \right) - \omega_S T_{\text{slack}} \\ & \text{s.t. } T(k+1) = \tau T(k) + \gamma e(k) + \rho T_a(k) \forall k \in \mathcal{K}_\delta \\ & e(k) \geq (i_{\text{total}}(k))^2 \quad \forall k \in \mathcal{K}_\delta \\ & i_{\text{total}}(k) = i_d(k) + \sum_{n=1}^N u_n(k) i_n^{\text{max}} \quad \forall k \in \mathcal{K}_\delta \\ & T(k+1) \leq T^{\text{max}} + T_{\text{slack}} \quad \forall k \in \mathcal{K}_\delta \\ & u_n(k) = 1 \quad \forall n \in \mathcal{Y}_k \forall k \in \mathcal{K}_\delta \\ & u_n(k) \leq u_n(k+1) \quad \forall n \in \mathcal{E}_1 \cup \mathcal{E}_2 \quad \forall k \in \mathcal{K}_\delta \\ & T(0) = T_{\text{meas}} \\ & \sum_{n \in \mathcal{E}_0} \sum_{m=0}^{\delta-1} u_n(m) = 0 \\ & u_n(k) \in \{0, 1\} \quad \forall n = 1, \dots, N \forall k \in \mathcal{K}_\delta \end{aligned}$$

Determine responses to packet requests from EV chargers:

$$\text{Resp}_n(k) = u_{\text{ch},n}^*(0) \forall n \quad \triangleright \text{From optimal solution.}$$

**End**

The optimal solutions of ADMM and ALADIN are nearly identical to the centralized solution. The convergence of the three iterative schemes in solving the OCP for the first (cold-start) time step of the receding-horizon simulation is shown in Fig. 6 (left). ALADIN significantly outperforms ADMM, which outperforms the Dual Decomposition. In Fig. 6 (right), the average solve time per time step over ten trials is shown for ALADIN and PEM as the number of EV agents increases and is well within the 180-s sample time. Note that the transformer parameters in Case Study 1 cause the OCP to become infeasible for 200 or more EVs. Thus, to test ALADIN and PEM for  $N > 100$ , the transformer's  $\gamma$  was scaled as a function of  $N$  to engender a consistent relative loading on the transformer as  $N$  increased. The ALADIN cold-start

TABLE II  
SIMULATION PARAMETERS FOR CASE STUDY 1

Variable	Value	Units	Source
<i>System parameters</i>			
$N$	100	EVs	[48], [49]
$K$	160	Timesteps	-
$M$	6	Segments	-
$\Delta t$	180	Seconds	[50], [51]
$\bar{T}_a(k)$	[16,18]	$^\circ\text{C}$	-
$c$	29.87		[9], [50], [51]
$i_d(k)$	[12.1,17.5]	kA	-
$T^{\text{max}}$	100	$^\circ\text{C}$	[5], [52]
$T_0$	70	$^\circ\text{C}$	-
$\gamma$	0.0131	$^\circ\text{C}/(\text{kA})^2$	[9], [50], [51]
$\tau$	0.9145		[9], [50], [51]
$\rho$	0.0855		[9], [50], [51]
$R$	240/8320		-
<i>Residential EV parameters</i>			
$s_{n,0}$	[0,70]	%	[53]
$i_n^{\text{max}}$	[12,80]	A	[48], [54]
$\alpha_n$	[80,90]	%	[55]
$\beta_n$	[40,100]	kWh	[48], [56]
$\bar{s}_n$	[75,100]	%	-
$\bar{k}_n$	[06:00,10:00]	Time	-
$q_n, r_n$	[0,50], 10		-

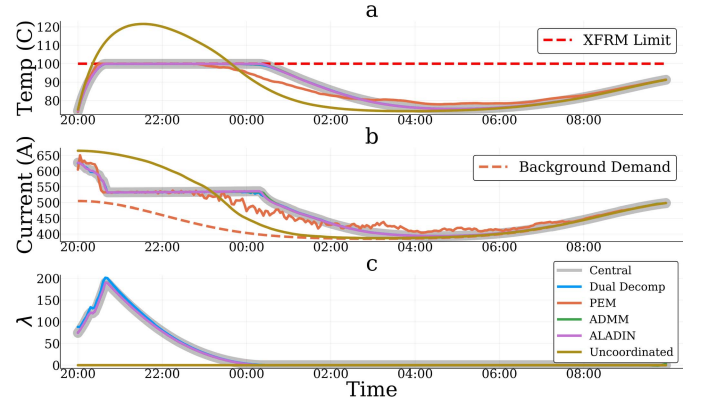


Fig. 5. Case Study 1 receding-horizon response. (a) Temperature response. (b) Total primary network current demanded from substation transformer and equal to reflected total secondary current ( $Ri_{\text{total}}(k)$ ). (c) Dual variable of (16).

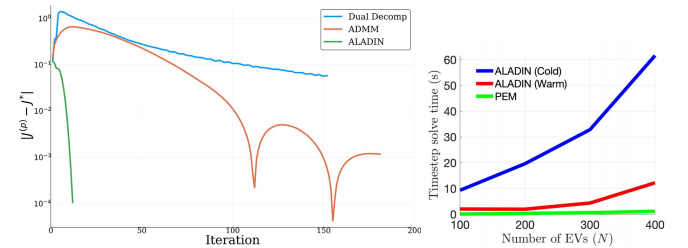


Fig. 6. Case Study 1 processing. Left: convergence for first (cold-start) time instance. Objective function values converging to centralized (optimal) value. Right: solve times for first (cold-start) and second (warm-start) time instances as  $N$  increases from 100 to 400 EVs.

case takes 10–11 iterations to converge, while the warm-start case takes just 2–3 iterations. The drop in solve time for ALADIN (warm) between  $N = 100$  and  $N = 200$  is due to the  $N = 100$  case taking three iterations, while the  $N = 200$  case takes just two iterations and is due to convergence tolerances. Beyond  $N = 400$ , ALADIN requires additional parameter

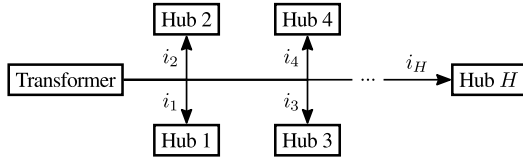


Fig. 7. Case Study 2 network of commercial EVC hubs, where the transformer's LV side is rated at  $V_{\text{pri}} = 13.2$  kV, while the commercial chargers are supplied at  $V_{\text{sec}} = 480$  V in the secondary network.

tuning to ensure consistent convergence; however, PEM was tested separately at  $N = 500$  (1.9 s) and  $N = 1000$  (14.5 s) vehicles. As expected, solving ALADIN's coordinator QP (at each iteration) and PEM's coordinator MIQCQP (once per time step) represents most of the solve time.

For the scenario in Case Study 1, privacy is important as individual EV owners may not be inclined to share information about their driving habits, such as time of arrival, departure, and/or SoC. Thus, since the ALADIN algorithm requires significant information transfer between EVs and coordinator, ALADIN is not well-suited in residential charging settings. However, due to its rapid convergence, ALADIN may be an ideal approach for solving EVC problems where privacy is less important and full information is available. For example, a fleet of commercial EVs located at central charging hubs within a large city fits those conditions (e.g., package or mail delivery vehicles with predetermined routes and arrival and departure times). Nonetheless, to account for known, but variable arrival/departure times of a commercial fleet would require that we significantly modify the algorithms presented in Case Study 1. To side-step this algorithm design challenge, we instead aggregate  $N$  EV agents with fixed energy and power limits into a single charging hub agent with variable energy and power limits, which is developed and presented in Section VI (Case Study 2). As will be shown, this slight modeling effort enables straightforward application of the previously developed distributed charging algorithms.

## VI. CASE STUDY 2: COMMERCIAL FLEET CHARGING

As commercial transportation becomes electrified, vehicle fleets will also benefit from charging control. In addition, the privacy of an individual vehicle in a commercial fleet is not a concern as one company owns and centrally plans the routes and times all EVs in their fleet. Furthermore, a large proportion of these fleets have predictable routes to and from a central depot, such a package or mail delivery trucks. These central depots or hubs represent local EVC centers or lots.

That is, due to mainly the known, but variable arrival and departure times of a fleet, the commercial/industrial EV hub setting is inherently different from the residential EV setting. Specifically, this difference requires modifying the presented ALADIN, ADMM, and dual decomposition algorithms to account for a plug-and-play implementation, which is technically less straightforward. However, instead of modifying the algorithms to match the problem, we will reformulate the problem by aggregating a hub's individual EVC agents, which have fixed energy and power limits, into a single hub charging

agent with variable energy and power limits that is a function of arrival and departures. Not only does this aggregate hub model approach enable scale in a commercial setting, but also it importantly allows us to directly consider the same algorithms developed previously for Case Study 1.

Thus, as illustrated in Fig. 7, we represent each hub  $h$  as a single agent in a system with  $H$  hubs and assume that internal to each hub is an algorithm that distributes allocated hub charging capacity to its  $N_h$  individual vehicles. Thus, the hub agent needs to model the aggregate available EV SoC and energy and current limits to ensure that the hub can meet the underlying, asynchronous EVC needs. Next, we leverage the EV model used in Case Study 1 to develop a dynamic model of a single hub charging agent and present the distributed optimal charging control problem for a collection of  $H$  hubs under a large MVA-scale substation transformer.

### A. Hub System Model

Define hub  $h \in \{1, \dots, H\}$  by a set of  $N_h$  assigned vehicles  $\mathcal{N}_h$ . Since we are aggregating different vehicles into a single hub, we will use physical rather than normalized battery capacity and will index each vehicle by its hub and vehicle indices  $(h, n)$ . Thus, each vehicle  $n \in \mathcal{N}_h$  has battery capacity  $E_{h,n}^{\text{max}}$  (in kWh). For arrival and departure times, in Case Study 1, all EVs arrived at the same time ( $k = 0$ ) and had a maximum time ( $\bar{k}_n$ ) by which they wanted to achieve a desired SoC ( $\bar{s}_n$ ). In Case Study 2, this concept is extended in that an EV is expected to arrive at time step  $\underline{k}_{h,n}$  with arrival energy  $\underline{s}_{h,n} E_{h,n}^{\text{max}}$  (in kWh) and is expected to leave at time step  $\bar{k}_{h,n}$  with desired minimum departure energy  $\bar{s}_{h,n} E_{h,n}^{\text{max}}$  (in kWh), that is,  $\bar{k}_{h,n}$  represent a physical departure time in Case Study 2 instead of the owner preference from Section II-C. Finally, the value  $\underline{s}_{h,n}$  ( $\bar{s}_{h,n}$ ) represents the vehicle's relative SoC at arrival (departure).

For each hub and each time step, we then define sets for arriving, parked, and departing vehicles

$$\begin{aligned} \text{Arrive}_h(k) &= \{n \in \mathcal{N}_h | k = \underline{k}_{h,n}\} \\ \text{Parked}_h(k) &= \{n \in \mathcal{N}_h | \underline{k}_{h,n} < k < \bar{k}_{h,n}\} \\ \text{Depart}_h(k) &= \{n \in \mathcal{N}_h | k = \bar{k}_{h,n}\} \end{aligned}$$

and calculate the arrival and departure energy trajectories

$$\begin{aligned} E_{h,\text{arrive}}(k) &= \sum_{n \in \text{Arrive}_h(k)} \underline{s}_{h,n} E_{h,n}^{\text{max}} \\ E_{h,\text{depart}}(k) &= \sum_{n \in \text{Depart}_h(k)} \bar{s}_{h,n} E_{h,n}^{\text{max}}. \end{aligned}$$

These trajectories define the amount of energy added and subtracted to hub  $h$  from the predicted vehicle arrivals and departures. From the parked vehicles in hub  $h$  at time  $k$ , we can also define the time-varying upper limits on energy and effective current:

$$\begin{aligned} E_h^{\text{max}}(k) &= \sum_{n \in \text{Parked}_h(k)} E_{h,n}^{\text{max}} \quad \text{and} \\ i_h^{\text{max}}(k) &= \sum_{n \in \text{Parked}_h(k)} i_{h,n}^{\text{max}}. \end{aligned}$$

Note that although the maximum current capacity of the charging facility would not change physically, the effective maximum current at time  $k$  is a function of the variable number of parked vehicles.

Finally, since vehicle  $n$  can depart from a hub  $h$  with more than its desired departure SoC  $\bar{s}_{h,n}E_{h,n}^{\max}$ , we need to account for the difference between the expected departing SoC and actually departing with up to 100% of SoC. Thus, the maximum additional energy that can depart hub  $h$  at time  $k$  is given by

$$E_{h,\Delta}^{\max}(k) = \sum_{n \in \text{Depart}_h(k)} (1 - \bar{s}_{h,n}) E_{h,n}^{\max}. \quad (19)$$

From these sets and trajectories, we can now form the hub energy dynamics and optimization.

### B. Hub Energy Dynamics and Bounds

The SoC for each hub at time  $k + 1$  is a function of the current delivered over time step  $k$ , the expected energy lost from departing vehicles, and the expected energy gained from arriving vehicles. The departed energy from each time step is the expected target SoC for departing vehicles plus any extra energy provided to bring (some) vehicles above required  $\bar{s}_{h,n}$ ,  $E_{h,\text{depart}} + E_{h,\Delta}$ . Overall, the model reads

$$E_h(k+1) = E_h(k) + \eta_h i_h(k) + E_{h,\text{arrive}}(k) - (E_{h,\text{depart}}(k) + E_{h,\Delta}(k)) \quad (20a)$$

$$0 \leq E_h(k) \leq E_h^{\max}(k) \quad (20b)$$

$$0 \leq E_{h,\Delta}(k) \leq E_{h,\Delta}^{\max}(k) \quad (20c)$$

$$0 \leq i_h(k) \leq i_h^{\max}(k). \quad (20d)$$

To illustrate the relationship between the EV model presented in Section II and that of the hub, we consider the simple case of a hub with a single EV (i.e.,  $N_h = 1$ ). Then, before arrival ( $k < \underline{k}_{h,1}$ ), the dynamics in (20a) are  $E_h(k+1) = 0$ . Upon arrival ( $k = \underline{k}_{h,1}$ ), (20a) becomes  $E_h(k+1) = \underline{s}_{h,1} E_{h,1}^{\max}$ , which is the usual initial state. While parked ( $\underline{k}_{h,1} < k < \bar{k}_{h,1}$ ), the dynamics revert to standard EV SoC dynamics in kWh units:  $E_h(k+1) = \underline{s}_{h,1} E_{h,1}^{\max} + \sum_{k=\underline{k}_{h,1}+1}^k \eta_h i_h(k)$ . Finally, upon departure ( $k = \bar{k}_{h,1}$ ), we get

$$E_h(k+1) = \underline{s}_{h,1} E_{h,1}^{\max} + \sum_{k=\underline{k}_{h,1}+1}^{\bar{k}_{h,1}} \eta_h i_h(k) - \bar{s}_{h,1} E_{h,1}^{\max} - E_{h,\Delta}(k)$$

where the left-hand side yields  $E_h(k+1) \equiv 0$  since the hub has no vehicle at time  $k+1$ . This means that the difference between realized and expected departing SoC is

$$\Rightarrow E_{h,\Delta}(k) = \left( \underline{s}_{h,1} E_{h,1}^{\max} + \sum_{k=\underline{k}_{h,1}+1}^{\bar{k}_{h,1}} \eta_h i_h(k) \right) - \bar{s}_{h,1} E_{h,1}^{\max}.$$

Since the positive term in the parenthesis is less than  $E_{h,1}^{\max}$

$$\Rightarrow E_{h,\Delta}(k) \leq (E_{h,1}^{\max}) - \bar{s}_{h,1} E_{h,1}^{\max} = (1 - \bar{s}_{h,1}) E_{h,1}^{\max} = E_{h,\Delta}^{\max}(k)$$

where the last equality is a direct application of (19). Finally, with  $E_{h,\Delta}(k) \geq 0$ , the hub will satisfy charging requirements,

if the problem is feasible. This description extends to  $N_h$  vehicles in the hub. Thus, across the arrival, parked, and departure phases of the hub, energy dynamics are captured with the the hub model in (20).

*Remark:* Note that the hub charging efficiency parameter  $\eta_h$  is assumed to be time-invariant (i.e., EVs charge with the same efficiency). However,  $\eta_h$  could be estimated based on a weighted combination of the efficiencies in  $\text{Parked}_h(k)$  or other simplifications [56].

### C. Objective Function With Hubs

The local hub objective function is similar to the one in the local (residential) EV scenario. However, since vehicles physically leave the hub, the hub loses energy with departures and there is no need to track 100% SoC for the entire hub. Thus, the hub seeks to minimize deviations of the predicted hub energy level from its maximum possible energy state, which is the sum of the energy capacities for all vehicles parked at time  $k$ . In addition, if possible, it is desirable to maximize the  $E_{h,\Delta}(k)$  terms as they allow the hub to exceed the minimum required energy levels. The weighting factor  $o_h$  determines how desirable oversupplying energy is relative to the weights of the other two terms ( $q_h$  and  $r_h$ ) and defines objective  $h$  as

$$J_h(\mathbf{i}_h, \mathbf{E}_h, \mathbf{E}_{h,\Delta}) = \sum_{k=1}^K q_h (E_h(k) - E_h^{\max}(k))^2 + r_h (i_h(k))^2 - o_h E_{h,\Delta}(k). \quad (21)$$

Thus, with this objective function and the hub model in (20), we formulate the centralized OCP for a system of hubs next.

### D. Centralized OCP With Hubs

With the same PWL approximation of the transformer model as in (12), we can combine the hub dynamics and objective function to yield a centralized hub OCP

$$\min \sum_{h=1}^H J_h(\mathbf{i}_h, \mathbf{E}_h, \mathbf{E}_{h,\Delta}) \quad (22a)$$

$$\text{s.t. } E_h(k+1) = E_h(k) + \eta_h i_h(k) + E_{h,\text{arrive}}(k) - (E_{h,\text{depart}}(k) + E_{h,\Delta}(k)) \quad (22b)$$

$$T(k+1) = \tau T(k) + \rho T_a(k) + \gamma \left( \Delta i \sum_{m=1}^M (2m-1) i_m^{\text{PW}}(k) \right) \quad (22c)$$

$$i_d(k) + \sum_{h=1}^H i_h(k) = \sum_{m=1}^M i_m^{\text{PW}}(k) \quad | \lambda(k) \quad (22d)$$

$$0 \leq E_{h,\Delta}(k) \leq E_{h,\Delta}^{\max}(k) \quad (22e)$$

$$0 \leq i_m^{\text{PW}}(k) \leq \Delta i \quad \forall m = 1, \dots, M \quad (22f)$$

$$0 \leq i_h(k) \leq i_h^{\max}(k) \quad (22g)$$

$$0 \leq E_h(k+1) \leq E_h^{\max}(k), \quad E_h(0) = E_{\text{meas},n} \quad (22h)$$

$$T(k+1) \leq T^{\max}, \quad T(0) = T_{\text{meas}} \quad (22i)$$

for all  $k = 0, \dots, K-1$  and  $h = 1, \dots, H$ .

TABLE III  
SIMULATION PARAMETERS FOR CASE STUDY 2

Variable	Value	Units
<i>System parameters</i>		
$H$	4	Hubs
$N_h$	100	EVs
$K$	240	Timesteps
$M$	15	Segments
$\Delta t$	180	Seconds
$\tilde{T}_a(k)$	[16,18]	$^{\circ}\text{C}$
$c$	29.87	-
$i_d(k)$	[52,64]	kA
$T^{\max}$	100	$^{\circ}\text{C}$
$T_0$	70	$^{\circ}\text{C}$
$\gamma; \tau; \rho$	{0.000524, 0.9145, 0.0855}	{ $^{\circ}\text{C}/(\text{kA})^2, -, -$ }
$R$	480/13200	
<i>Commercial EV hub parameters</i>		
$i_h^{\max}$	[200,1000]	A
$\alpha_n$	[80,90]	%
$E_{h,n}^{\max}$	[100,600]	kWh
$s_{h,n}$	[10,40]	%
$\bar{s}_{h,n}$	[80,100]	%
$k_{h,n}$	[20:00, 03:00]	-
$\bar{k}_{h,n}$	[04:00, 07:00]	-
$q_h, r_h, o_h$	[0.1,200], 10, 100	-

### E. Noncentralized Hub Formulation

A similar decomposition from Case Study 1 can be used to form the partial Lagrangian

$$\begin{aligned} \mathcal{L} & \left( \{\mathbf{i}_h\}_{h=1}^H, \{\mathbf{E}_h\}_{h=1}^H, \{i_m^{\text{PW}}\}_{m=1}^M, \lambda \right) \\ & = \sum_{h=1}^H J_h(\mathbf{i}_h, \mathbf{E}_h) + \lambda^{\top} \left( \mathbf{i}_d + \sum_{h=1}^H \mathbf{i}_h - \sum_{m=1}^M \mathbf{i}_m^{\text{PW}} \right) \\ & = \sum_{h=1}^H \left( J_h(\mathbf{i}_h, \mathbf{E}_h) + \lambda^{\top} \mathbf{i}_h \right) + \lambda^{\top} \left( \mathbf{i}_d - \sum_{m=1}^M \mathbf{i}_m^{\text{PW}} \right). \end{aligned}$$

Now, the developed hub model exactly enables the primal problem formulation to attain the same form as in Case Study 1 and, thus, we can use the same ALADIN, ADMM, and dual decomposition algorithms from Section IV. This is despite the time-varying arrivals and departures of the individual vehicles in the hubs.

### F. Simulation Setup for Case Study 2

A hub model simulation was conducted for  $H = 4$  hubs with  $N_h = 100$  EVs in each hub. The distribution-level transformer in this scenario is a large 100-MVA transformer with a primary network voltage rating of  $V_{\text{pri}} = 13.2$  kV. Within the hubs, the secondary network supplies commercial chargers with rms voltage at  $V_{\text{sec}} = 480$  V. Since this scenario focuses on commercial vehicles, the battery capacities have been sized accordingly at 100, 200, or 600 kWh with charging rates between 96 and 480 kVA. For simplicity, a constant background load of 25–30 MVA is used. Table III presents the relevant parameters for Case Study 2.

### G. Discussion of Case Study 2 Results

The central and uncoordinated results can be seen compared with the optimization algorithms solutions in Fig. 8.

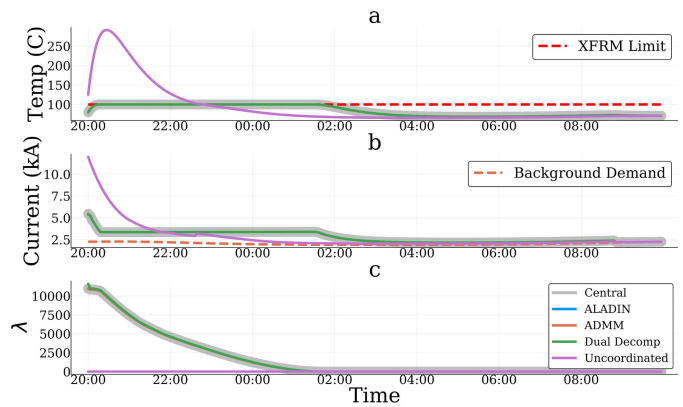


Fig. 8. Case Study 2 results for allocating current capacity to hubs. (a) Temperature response. (b) Total primary network current demanded from transformer and equal to reflected total secondary current ( $Ri_{\text{total}}(k)$ ). (c) Dual variable.

Once again, ALADIN and ADMM perform well and match the central solution. Unlike in the residential scenario, PEM is not suitable for managing ON/OFF charging packets for hubs representing the equivalent of up to 100 EVs charging coincidentally, which begets large (bulky) demands on the transformer and makes temperature regulation challenging. Thus, PEM is not part of the commercial hub scenario, except as the possible intrahub EVC coordinator that ensures that a hub's aggregate demand is below its optimized static current capacity allocation. The comparison of the four distributed methods in Case Studies 1 and 2 is next.

## VII. COMPARISON OF DISTRIBUTED METHODS

### A. Privacy, Performance, and Processing

In Sections V and VI, the results of a receding-horizon implementation of the OCP is presented for each case study. In this section, we discuss how these methods are performed and compare each method in terms of privacy (communication), performance (optimality), and processing (computation).

1) *Privacy*: Table IV shows the information communicated between the EVs, coordinator, and transformer. The most valuable information from a consumer standpoint is the current and SoC schedules. While both dual ascent and ADMM transfer the current schedule to the coordinator, the coordinator only uses the sum of the current schedules, so this sensitive information could be passed through a third party and aggregated first. However, in ALADIN, the individual current schedule is used in the coordinator problem as well as in the gradient. To approximate information requirements per time step, consider an average number of iterations, a population of  $N = 100$  EV chargers, and a prediction horizon of 160 time steps. Then, breaking these numbers into the data communicated per time step and per EV, we get 32 bits for PEM, 21 Mb for dual decomposition, 3 Mb for ADMM, and 0.6 Mb for ALADIN, that is, PEM and ALADIN require far less data to be communicated than the other two methods.

2) *Performance*: A summary of the performance of the four distributed methods is shown in Table V. Specifically,

TABLE IV  
SUMMARY OF DISTRIBUTED METHODS—INFORMATION SHARING

From-to	ALADIN	Dual Ascent / ADMM	PEM
EV to Coordinator	$\mathbf{i}_n^{(p)}, \mathbf{g}_{i,n}^{(p)}, \mathbf{g}_{s,n}^{(p)}, \mathbf{C}_{i,n}^{(p)}, \mathbf{C}_{i,n}^{(p)}, \mathbf{C}_{s,n}^{(p)}, \mathbf{C}_{s,n}^{(p)}$	$\mathbf{i}_n^{(p)}$	$\text{Req}_n(k)$
Transformer to Coordinator	$\sum_{m=1}^M (\mathbf{i}_m^{PW})^{(p)}, \mathbf{g}_{i,PW}^{(p)}, \mathbf{g}_t^{(p)}, \mathbf{C}_z^{(p)}, \mathbf{C}_t^{(p)}, \mathbf{C}_t^{(p)}$	$\sum_{m=1}^M (\mathbf{i}_m^{PW})^{(p)}$	$T(k)$
Coordinator to EV	$\lambda^{(p)}, \mathbf{V}_{i,n}^{(p)}, \mathbf{V}_{s,n}^{(p)}$	$\lambda^{(p)}, (\mathbf{V}_{i,n}^{(p)})$	$\text{Resp}_n(k)$
Coordinator to Transformer	$\lambda^{(p)}, \mathbf{V}_t^{(p)}, \mathbf{V}_{i,PW}^{(p)}$	$\lambda^{(p)}, (\mathbf{V}_{i,PW}^{(p)})$	-

TABLE V  
SUMMARY OF DISTRIBUTED METHODS—PERFORMANCE

Method	2-Norm Current Schedule		2-Norm Lambda	
	Case Study 1	Case Study 2	Case Study 1	Case Study 2
ALADIN	1e1	2e2	6e-4	4e-3
ADMM	8e1	3e2	4e-3	3e-2
Dual Decomposition	2e2	3e3	6e-2	8e-1
PEM	5e3	-	-	-

it compares the two-norm of the difference between the centralized method's optimal current schedules ( $\mathbf{i}_n^*$ ) and dual variables ( $\lambda^*$ ) and the optimized values from the distributed methods. In both case studies, ALADIN and ADMM performed well as their solutions achieved optimality. Dual decomposition does not converge completely in the allotted time and performs worse as a result. The PEM coordinator focuses on the feasibility of local and transformer problems with device-driven priorities and has no optimality guarantees; therefore, the difference in the current schedules is more pronounced for Case Study 1.

3) *Processing*: The computational efficiency of the methods is shown in Table VI. The average solver time metric describes the average time it takes the algorithm to process for each time step. This number is not necessarily proportional to the average number of iterations shown in the second column as some algorithms require more processing per iteration. The PEM implementation requires the least processing as it is an iteration-free approach. ALADIN is the next quickest followed by ADMM and dual decomposition. In the implementation, the algorithms have a constraint on the number of iterations due to the duration of each time step. Increasing the number of EVs in the simulation would likely have a similar number of iterations per time step; however, the performance especially for dual decomposition and ADMM would decrease. It is worth noting that the stopping criteria were different for Case Studies 1 and 2. In addition, the centralized results are only meant to be representative at the proposed scale as direct load control does not scale well in practice when the number of agents (EVs or hubs) or the prediction horizon increases.

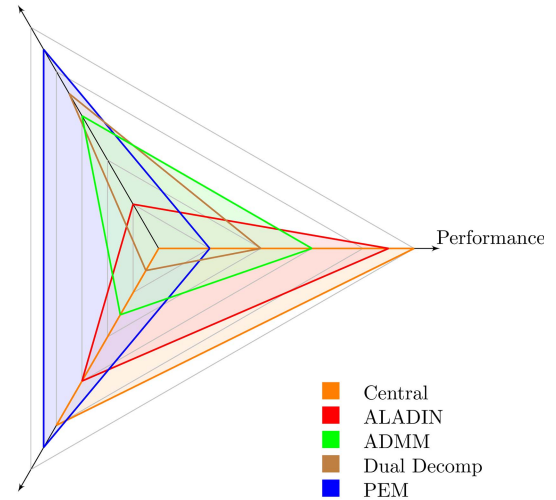
### B. Summary of Results

A qualitative summary of the differences in the distributed methods is shown in Fig. 9. The central formulation gives the

TABLE VI  
SUMMARY OF DISTRIBUTED METHODS—PROCESSING

Method	Average Solver Time/Iter. (Sec)		Average Iter. to Converge	
	Case Study 1	Case Study 2	Case Study 1	Case Study 2
Central	3e-1	4e-2	1	1
ALADIN	2e-1	4e-2	1.9	1.4
ADMM	8e-3	1e-2	6.9	18
Dual Decomposition	2e-3	5e-3	284	1000
PEM	6e-2	-	1	-

Privacy



Processing

Fig. 9. Qualitative relative ranking of the different EVC control methods.

optimal solution quickly but gives no privacy and has a high communication overhead at scale. Dual decomposition and ADMM improve on data privacy but see a significant decrease in the performance and computational efficiency. ALADIN shows the best performance out of the distributed methods but sacrifices privacy. PEM contrasts interestingly with central and offers maximum privacy and speed but without optimality guarantees.

### C. Selecting a Suitable Distributed Method

For the scenario in Case Study 1, privacy is important as residential EV owners should not need to share their private driving information. Using ALADIN, the coordinator knows the gradients, which are a scaled version of the current schedule and are sensitive data. Due to the large amount of information being shared with the ALADIN algorithm, this may not be the best approach even though it shows the best performance. Thus, ADMM or PEM is well-suited for residential fleets. For commercial fleets, such as in Case Study 2, where data privacy is less of a priority, ALADIN is a powerful option. Clearly, for a general setting, the order of priorities must be decided before deciding on a specific method.

## VIII. CONCLUSION AND FUTURE WORK

Utilities and other entities in the energy industry will soon have to consider the impacts of increased adoption of

EVs. Uncoordinated charging could cause overloading of grid transformers as the penetration of EVs increases. We have developed two novel distributed control strategies (ALADIN and PEM) and shown that they could be implemented to avoid costly upgrades of transformers. We have compared the tradeoff of these novel methods to conventional algorithms (ADMM and dual decomposition) in the areas of privacy (communication), performance (optimality), and processing (computation time). Finally, a novel EVC aggregation hub model was developed that models  $N$  commercial EVs with fixed current and energy limits into a single resource with variable current and energy limits when a good arrival/departure forecast is available. This hub model effectively extends the presented distributed algorithms for fixed EV population to populations with variable EV populations (defined by forecast arrival/departure rates).

Based on two different case studies (residential and commercial), we found that the proposed and novel suboptimal, but privacy-preserving algorithm PEM might be ideal for an application where privacy is valued, such as a residential EVC. On the other hand, in a commercial fleet setting with multiple charging hubs, where performance is a priority, ALADIN represents a good choice.

The EVC problem presented herein is deterministic, implemented in a synchronous fashion, and does not explore control objectives that incentivize V2G operation of EVs. In addition, the transformer is assumed to be operating with an ideal model under balanced loading. Thus, future directions of research will explore stochastic, robust, and asynchronous EVC implementations that could permit peer-to-peer sharing of resources via different market signals and more general transformer models and operations. Furthermore, since future control methods will require more than EVs to be coordinated and incorporate ac grid reliability constraints, access to and the role of (private) information will be critical. Within this context, we are interested to extend ALADIN and PEM to consider other types of DERs for demand management, additional (coupling and unbalanced) grid constraints via ac OPF formulation, and investigate the effects of negative background demand due to solar photovoltaic (PV). By incorporating utility network information into the control algorithms, it also becomes critical to consider the role of cybersecurity, which is an important aspect of data privacy.

## APPENDIX A - PROOF OF THEOREM 1

The tightness proof for the relaxed transformer dynamics in Theorem 1 relies on the KKT analysis. Thus, we first need to define the primal constraints and dual variables of the relevant SOCP formulation of (8) along with the KKT stationarity conditions. These are presented before the proof.

### A. Primal Constraints and Dual Variables

Consider the primal SOCP constraints from (8) with the SoC limits removed as they are not needed for the conditions in Theorem 1. For all  $k \in \mathcal{K} \doteq \{0, \dots, K - 1\}$  and  $n \in \mathcal{N} \doteq \{1, \dots, N\}$ , the following constraints define primal feasibility

and dual variables after |:

$$0 = T(k + 1) - \tau T(k) - \eta e(k), \quad |\lambda_T^{k+1} \in \mathbb{R} \quad \forall k \quad (23a)$$

$$0 = s_n(k + 1) - s_n(k) - \eta n i_n(k), \quad |\lambda_{s_n}^{k+1} \in \mathbb{R} \quad \forall k \quad \forall n \quad (23b)$$

$$0 = i_{\text{total}}(k) - i_d(k) - \sum_{n=1}^N i_n(k), \quad |\lambda_c^k \in \mathbb{R} \quad \forall k \quad (23c)$$

$$0 \geq T(k + 1) - T^{\max}, \quad |\mu_T^{k+1} \geq 0 \quad \forall k \quad (23d)$$

$$0 \geq (i_{\text{total}}(k))^2 - e(k), \quad |\mu_e^k \geq 0 \quad \forall k \quad (23e)$$

$$0 \geq i_n(k) - i_n^{\max}, \quad |\bar{\mu}_{i_n}^k \geq 0 \quad \forall k \quad \forall n \quad (23f)$$

$$0 \geq 0 - i_n(k), \quad |\underline{\mu}_{i_n}^k \geq 0 \quad \forall k \quad \forall n \quad (23g)$$

$$0 \geq \bar{s}_n - s_n(\bar{k}_n + 1), \quad |\bar{\mu}_{s_n}^{\bar{k}_n+1} \geq 0 \quad \forall n \quad (23h)$$

where the last constraint is the QoS guarantee that ensures that vehicle  $n$  achieves at least an SoC of  $\bar{s}_n$  by no later than time  $\bar{k}_n + 1$ . Without loss of generality, we can also set  $i_d(k) \equiv 0$  and assume  $s_n(0) > 0$ .

### B. KKT Stationarity Conditions

If we assume Slater's constraint qualification holds,<sup>5</sup> the stationarity condition  $\nabla_{x(k)} \mathcal{L}(x, \lambda, \mu) = 0$  has to hold for each variable  $x$  at time step  $k$ , which gives

$$\nabla_{T(k+1)} \mathcal{L} \Rightarrow \lambda_T^{k+1} = \tau \lambda_T^{k+2} - \mu_T^{k+1} \quad (24a)$$

$$\nabla_{T(k)} \mathcal{L} \Rightarrow \lambda_T^k = -\mu_T^k \quad (24b)$$

$$\nabla_{e(k)} \mathcal{L} \Rightarrow 0 = -\eta \lambda_T^{k+1} - \mu_e^k \quad (24c)$$

$$\nabla_{i_{\text{total}}(k)} \mathcal{L} \Rightarrow 0 = \lambda_c^k + 2\mu_e^k i_{\text{total}}(k) \quad (24d)$$

$$\nabla_{i_n(k)} \mathcal{L} \Rightarrow 0 = 2r_n i_n(k) - \eta n \lambda_{s_n}^{k+1} - \lambda_c^k + \bar{\mu}_{i_n}^k - \underline{\mu}_{i_n}^k \quad (24e)$$

$$\nabla_{s_n(k+1)} \mathcal{L} \Rightarrow \lambda_{s_n}^{k+1} = \lambda_{s_n}^{k+2} + 2q_n(1 - s_n(k + 1)) \quad (24f)$$

$$\nabla_{s_n(\bar{k}_n+1)} \mathcal{L} \Rightarrow \lambda_{s_n}^{\bar{k}_n+1} = \lambda_{s_n}^{\bar{k}_n+2} + 2q_n(1 - s_n(\bar{k}_n + 1)) + \bar{\mu}_{s_n}^{\bar{k}_n+1} \quad (24g)$$

$$\nabla_{s_n(K)} \mathcal{L} \Rightarrow \lambda_{s_n}^K = 2q_n(1 - s_n(K)). \quad (24h)$$

Before we can complete the proof, we need help from three technical lemmas that employ the primal and dual relations.

*Lemma 1:* At optimality, the dual variable,  $\mu_e^k$ , associated with relaxed quadratic constraint (23e), satisfies  $\mu_e^l \geq \mu_e^k$  for all  $l \leq k$ . Specifically, if (23e) is strictly active at time step  $k$ , then it is strictly active for all prior time steps.

*Proof:* From recursion on (24a) and (24b), we have

$$\lambda_T^{k+1} = - \sum_{t=k+1}^K \tau^{t-k-1} \mu_T^t \quad (25)$$

for all  $k$ , where  $\mu_T^{k+1} \geq 0 \quad \forall k \in \mathcal{K}$ . Substituting  $\lambda_T^{k+1}$  from (25) into (24c), we have that for all  $l \leq k$

$$\mu_e^l = \eta \sum_{t=l+1}^K \tau^{t-l-1} \mu_T^t \quad (26)$$

$$= \eta \left( \sum_{t=l+1}^k \tau^{t-l-1} \mu_T^t + \sum_{t=k+1}^K \tau^{t-k-1} \mu_T^t \right) \geq \mu_e^k. \quad (27)$$

<sup>5</sup>This is reasonable for the SOCP formulation and equivalent to the existence of a strictly feasible solution where the transformer temperature is not at its limit at all times, i.e., we have some flexibility in the system.

Thus, if  $\mu_e^k > 0 \Rightarrow \mu_e^l > 0 \forall l \leq k$ , this concludes the proof.  $\square$

*Lemma 2:* From (24f) and (24h) and recursion on  $k$ , it is trivial to show that for all  $k$

$$\lambda_{s_n}^{k+1} = \sum_{t=k+1}^K 2q_n(1 - s_n(t)) + I_{\bar{k},k} \bar{\mu}_{s_n}^{\bar{k}_n+1} \quad (28)$$

where  $I_{\bar{k},k} = 1$  if  $k \leq \bar{k}_n$  and  $I_{\bar{k},k} = 0$  otherwise.

*Lemma 3:* Since  $i_n(k) \geq 0$ , the sequence  $\{s_n(k)\}_{k=1}^K$  defined by (23b) is clearly nondecreasing for all  $n \in \mathcal{N}$ , that is,  $1 \geq s_n(k+1) \geq s_n(k) \geq s_n(0)$  for all  $k \in \mathcal{K}$ .

### C. Proof of Theorem 1

*Proof:* (Direct) From Lemma 1, we just need to show that  $\mu_e^k > 0$ . Thus, first, consider (24e) for time step  $k$  and substitute for  $\lambda_c^k$  with (24d) and  $\lambda_{s_n}^{k+1}$  with Lemma 2, which yields

$$0 = 2r_n i_n(k) - \eta_n \left( 2q_n \sum_{t=k+1}^K (1 - s_n(t)) + I_{\bar{k},k} \bar{\mu}_{s_n}^{\bar{k}_n+1} \right) + 2\mu_e^k i_{\text{total}}(k) + \bar{\mu}_{i_n}^k - \underline{\mu}_{i_n}^k$$

and  $\mu_e^k$  to the left-hand side gives

$$2\mu_e^k i_{\text{total}}(k) = \eta_n \left( 2q_n \sum_{t=k+1}^K (1 - s_n(t)) + I_{\bar{k},k} \bar{\mu}_{s_n}^{\bar{k}_n+1} \right) + \underline{\mu}_{i_n}^k - 2r_n i_n(k) - \bar{\mu}_{i_n}^k. \quad (29)$$

Since the transformer is overloaded due to excessive demand,  $i_{\text{total}}(l) > 0$ . Thus, we just need to show that RHS is strictly positive. Before doing so, we first simplify the notation by defining  $\alpha_n(k, \bar{k}_n) \doteq \eta_n I_{\bar{k},k} \bar{\mu}_{s_n}^{\bar{k}_n+1} + \underline{\mu}_{i_n}^k - \bar{\mu}_{i_n}^k$  where  $\alpha_n(k, \bar{k}_n) \geq 0$  since  $i_n(k) < i_n^{\max}$ . Clearly, if  $r_n = 0$ , the proof is complete for  $s_n(k+1) < 1$ . However, for  $r_n > 0$ , we need to consider the ratio  $q_n/r_n$ . Thus, we will use (23b) and replace  $i_n(k)$  with  $(1/\eta_n)(s_n(k+1) - s_n(k))$  in (29)

$$\begin{aligned} 2\mu_e^k i_{\text{total}}(k) &= 2q_n \eta_n \sum_{t=k+1}^K (1 - s_n(t)) \\ &\quad - 2 \frac{r_n}{\eta_n} (s_n(k+1) - s_n(k)) + \alpha_n(k, \bar{k}_n) \\ 2\mu_e^k i_{\text{total}}(k) &\geq 2q_n \eta_n \left( (1 - s_n(k+1)) + \sum_{t=k+2}^K (1 - s_n(t)) \right) \\ &\quad - 2 \frac{r_n}{\eta_n} (s_n(k+1) - s_n(k)) \end{aligned}$$

where the inequality is due to  $\alpha_n(k, \bar{k}_n) \geq 0$ . Further reductions show that  $2\mu_e^k i_{\text{total}}(k)$

$$\begin{aligned} &\geq 2q_n \eta_n (1 - s_n(k+1)) - 2 \frac{r_n}{\eta_n} (s_n(k+1) - s_n(k)) \\ &\geq 2 \frac{r_n}{\eta_n} \left( \frac{q_n}{r_n} \eta_n^2 (1 - s_n(k+1)) - s_n(k+1) + s_n(0) \right) \\ &= 2 \frac{r_n}{\eta_n} (M_n + s_n(0) - (M_n + 1)s_n(k+1)) \end{aligned}$$

where the last inequality is due to Lemma 3. For  $r_n > 0$  and  $s_n(k+1) < (M_n + s_n(0))/(M_n + 1)$ , the RHS is strictly

positive, which ensures that  $\mu_e^k > 0$ . Finally, from Lemma 1, we have  $\mu_e^l \geq \mu_e^k > 0 \forall l \leq k$ , which completes the proof.  $\square$

## APPENDIX B - PROOF OF COROLLARY 1

*Proof:* This proof has two parts.

- 1) Proving if  $k$  is largest time step to satisfy  $\mu_e^k > 0$ , then  $\mu_T^{k+1} > 0$  and  $\mu_T^m = 0 \forall m > k+1$ . Recall that in (26), since  $\eta, \tau > 0$  and  $\mu_T^t \geq 0$ , if  $\mu_e^k > 0$ , then  $\exists m > k$  such that  $\mu_T^{m+1} > 0$ . Now, assume  $m > k+1$ , and then

$$\mu_e^m = \eta \sum_{t=m+1}^K \tau^{t-m-1} \mu_T^t \Rightarrow \mu_e^m > 0.$$

However, since  $m > k$  that contradicts with  $k$  being the largest integer for which  $\mu_e^k > 0$  and, thus,  $\mu_T^m = 0 \forall m > k+1$  and  $k+1$  is the last instance of  $\mu_T^{k+1} > 0$ , which implies that  $T(k+1) = T^{\max}$ .

- 2) Proving if  $k+1$  is last time step with  $\mu_T^{k+1} > 0$ , then  $\mu_e^k > 0$ . If  $k+1$  is the last instance of  $\mu_T^{k+1} > 0$ , then  $\mu_e^l > 0 \forall l \leq k$  and, thus,  $k$  is the largest integer for which  $\mu_e^k > 0$  and  $e(k) = (i_{\text{total}}(k))^2$ . This completes the proof.  $\square$

Note that in a practical setting, where optimality of EVC control is not critical, a practitioner could circumvent the complexity of the convex relaxation by augmenting objective function (8a) with a temperature deviation term  $-\epsilon(T^{\max} - T(k+1))$  for arbitrarily small  $\epsilon > 0$ . This incentivizes temperature trajectories far from the temperature limit by embedding a  $-\epsilon$  into the RHS of (24a) and (24b), which guarantees that  $\lambda_T^{k+1} < 0 \forall k \in \mathcal{K}$ . From (24c), this yields  $\mu_e^k > 0 \forall k$ , which ensures that the convex relaxation is tight for all time steps, regardless of transformer or fleet conditions, and  $q_n/r_n$  ratios. The practical impact of using this approach is that for larger  $\epsilon > 0$ , the EV optimal charging schedule embodies a utility-centric, valley-filling policy [23], [25], which competes with that of the QoS-centric objective in (8a) and may negatively impact EV customer satisfaction.

## REFERENCES

- [1] J. Hodges. (Mar. 2018). *Electric Car Costs Set to Fall*. [Online]. Available: <https://www.bloomberg.com/news/articles/2018-03-22/electric-car-costs-set-to-fall>
- [2] N. Zart. (Apr. 2018). *Do Electric Vehicles Have Better Overall Safety? Part 2*. [Online]. Available: <https://cleantechnica.com/2018/04/01/do-electric-vehicles-have-better-overall-safety-part-2/>
- [3] E. W. Wood, C. L. Rames, A. Bedir, N. Crisostomo, and J. Allen, "California plug-in electric vehicle infrastructure projections: 2017–2025-future infrastructure needs for reaching the state's zero emission-vehicle deployment goals," Nat. Renew. Energy Lab., Golden, CO, USA, Tech. Rep. NREL/TP-5400-70893, Mar. 2018.
- [4] A. D. Hilshey, P. D. H. Hines, P. Rezaei, and J. R. Dowds, "Estimating the impact of electric vehicle smart charging on distribution transformer aging," *IEEE Trans. Smart Grid*, vol. 4, no. 2, pp. 905–913, Jun. 2013.
- [5] *IEEE Guide for Loading Mineral-Oil-Immersed Transformers*, Standard C57.91-2011, 2012.
- [6] B. C. Lesieutre, W. H. Hagman, and J. L. Kirtley, "An improved transformer top-oil temperature model for use in an online monitoring and diagnostic system," *IEEE Power Eng. Rev.*, vol. 17, no. 1, p. 50, Jan. 1997.
- [7] D. J. Tylavsky, Q. He, G. A. McCulla, and J. R. Hunt, "Sources of error in substation distribution transformer dynamic thermal modeling," *IEEE Trans. Power Del.*, vol. 15, no. 1, pp. 178–185, Jan. 2000. [Online]. Available: <http://ieeexplore.ieee.org/document/847248/>

- [8] Q. He, J. Si, and D. J. Tylavsky, "Prediction of top-oil temperature for transformers using neural networks," *IEEE Trans. Power Del.*, vol. 15, no. 4, pp. 1205–1211, Oct. 2000. [Online]. Available: <http://ieeexplore.ieee.org/document/891504/>
- [9] A. Seier, P. D. H. Hines, and J. Frolik, "Data-driven thermal modeling of residential service transformers," *IEEE Trans. Smart Grid*, vol. 6, no. 2, pp. 1019–1025, Mar. 2015.
- [10] I. Daminov, R. Rigo-Mariani, R. Caire, A. Prokhorov, and M.-C. Alvarez-Héroult, "Demand response coupled with dynamic thermal rating for increased transformer reserve and lifetime," *Energies*, vol. 14, no. 5, p. 1378, Mar. 2021. [Online]. Available: <https://www.mdpi.com/1996-1073/14/5/1378>
- [11] D. K. Molzahn *et al.*, "A survey of distributed optimization and control algorithms for electric power systems," *IEEE Trans. Smart Grid*, vol. 8, no. 6, pp. 2941–2962, Nov. 2017.
- [12] D. P. Bertsekas and J. N. Tsitsiklis, *Parallel and Distributed Computation: Numerical Methods*, vol. 23. Englewood Cliffs, NJ, USA: Prentice-Hall, 1989.
- [13] A. Nedić, A. Olshevsky, and S. Wei, "Decentralized consensus optimization and resource allocation," in *Large-Scale and Distributed Optimization*. Cham, Switzerland: Springer, 2018, pp. 247–287.
- [14] R. Scattolini, "Architectures for distributed and hierarchical model predictive control—A review," *J. Process Control*, vol. 19, no. 5, pp. 723–731, May 2009.
- [15] A. Ghavami, K. Kar, and A. Gupta, "Decentralized charging of plug-in electric vehicles with distribution feeder overload control," *IEEE Trans. Autom. Control*, vol. 61, no. 11, pp. 3527–3532, Nov. 2016.
- [16] O. Ardakanian, S. Keshav, and C. Rosenberg, "Real-time distributed control for smart electric vehicle chargers: From a static to a dynamic study," *IEEE Trans. Smart Grid*, vol. 5, no. 5, pp. 2295–2305, Sep. 2014.
- [17] R. Carli and M. Dotoli, "A decentralized control strategy for optimal charging of electric vehicle fleets with congestion management," in *Proc. IEEE Int. Conf. Service Oper. Logistics, Inform. (SOLI)*, Sep. 2017, pp. 63–67.
- [18] H. Fan, C. Duan, C. Zhang, L. Jiang, C. Mao, and D. Wang, "ADMM-based multiperiod optimal power flow considering plug-in electric vehicles charging," *IEEE Trans. Power Syst.*, vol. 33, no. 4, pp. 3886–3897, Jul. 2018.
- [19] X. Zhou, P. Wang, and Z. Gao, "ADMM-based decentralized charging control of plug-in electric vehicles with coupling constraints in distribution networks," in *Proc. 37th Chin. Control Conf. (CCC)*, Jul. 2018, pp. 2512–2517.
- [20] J. Rivera, P. Wolfrum, S. Hirche, C. Goebel, and H.-A. Jacobsen, "Alternating direction method of multipliers for decentralized electric vehicle charging control," in *Proc. 52nd IEEE Conf. Decis. Control*, Dec. 2013, pp. 6960–6965.
- [21] W.-J. Ma, V. Gupta, and U. Topcu, "On distributed charging control of electric vehicles with power network capacity constraints," in *Proc. Amer. Control Conf. (ACC)*, Jun. 2014, pp. 4306–4311.
- [22] S. Weckx, R. D'Hulst, B. Claessens, and J. Driesensam, "Multi-agent charging of electric vehicles respecting distribution transformer loading and voltage limits," *IEEE Trans. Smart Grid*, vol. 5, no. 6, pp. 2857–2867, Nov. 2014.
- [23] M. Liu, P. K. Phanivong, Y. Shi, and D. S. Callaway, "Decentralized charging control of electric vehicles in residential distribution networks," *IEEE Trans. Control Syst. Technol.*, vol. 27, no. 1, pp. 266–281, Jan. 2019.
- [24] Y. Zhou, R. Kumar, and S. Tang, "Incentive-based distributed scheduling of electric vehicle charging under uncertainty," *IEEE Trans. Power Syst.*, vol. 34, no. 1, pp. 3–11, Jan. 2019.
- [25] Z. Ma, D. S. Callaway, and I. A. Hiskens, "Decentralized charging control of large populations of plug-in electric vehicles," *IEEE Trans. Control Syst. Technol.*, vol. 21, no. 1, pp. 67–78, Jan. 2013.
- [26] L. Gan, U. Topcu, and S. H. Low, "Optimal decentralized protocol for electric vehicle charging," *IEEE Trans. Power Syst.*, vol. 28, no. 2, pp. 940–951, May 2013.
- [27] X. Huang, C. Xu, P. Wang, and H. Liu, "LNSC: A security model for electric vehicle and charging pile management based on blockchain ecosystem," *IEEE Access*, vol. 6, pp. 13565–13574, 2018.
- [28] F. Knirsch, A. Unterweger, and D. Engel, "Privacy-preserving blockchain-based electric vehicle charging with dynamic tariff decisions," *Comput. Sci.-Res. Develop.*, vol. 33, nos. 1–2, pp. 71–79, Feb. 2018, doi: [10.1007/s00450-017-0348-5](https://doi.org/10.1007/s00450-017-0348-5).
- [29] B. Houska, J. Frasch, and M. Diehl, "An augmented Lagrangian based algorithm for distributed nonconvex optimization," *SIAM J. Optim.*, vol. 26, no. 2, pp. 1101–1127, Jan. 2016, doi: [10.1137/140975991](https://doi.org/10.1137/140975991).
- [30] P. Rezaei, J. Frolik, and P. D. H. Hines, "Packetized plug-in electric vehicle charge management," *IEEE Trans. Smart Grid*, vol. 5, no. 2, pp. 642–650, Mar. 2014.
- [31] M. Almassalkhi, J. Frolik, and P. Hines, "Packetized energy management: Asynchronous and anonymous coordination of thermostatically controlled loads," in *Proc. Amer. Control Conf. (ACC)*, May 2017, pp. 1431–1437.
- [32] M. Almassalkhi, L. D. Espinosa, P. D. H. Hines, J. Frolik, S. Paudyal, and M. Amini, *Asynchronous Coordination of Distributed Energy Resources With Packetized Energy Management*. New York, NY, USA: Springer, 2018, pp. 333–361.
- [33] L. A. D. Espinosa and M. Almassalkhi, "A packetized energy management macromodel with quality of service guarantees for demand-side resources," *IEEE Trans. Power Syst.*, vol. 35, no. 5, pp. 3660–3670, Sep. 2020, doi: [10.1109/TPWRS.2020.2981436](https://doi.org/10.1109/TPWRS.2020.2981436).
- [34] H. Chen, Z. Guo, Y. Xin, Y. Zhao, and Y. Jia, "Coordination of PEV charging across multiple stations in distribution networks using aggregate PEV charging load model," in *Proc. Int. Smart Cities Conf. (ISCC)*, Sep. 2017, pp. 1–5.
- [35] Z. Wei, Y. Li, Y. Zhang, and L. Cai, "Intelligent parking garage EV charging scheduling considering battery charging characteristic," *IEEE Trans. Ind. Electron.*, vol. 65, no. 3, pp. 2806–2816, Mar. 2018.
- [36] Y. Ota, H. Taniguchi, H. Suzuki, J. Baba, and A. Yokoyama, "Aggregated storage strategy of electric vehicles combining scheduled charging and V2G," in *Proc. ISGT*, Feb. 2014, pp. 1–5.
- [37] A. M. Jenkins, C. Patsios, P. Taylor, O. Olabisi, N. Wade, and P. Blythe, "Creating virtual energy storage systems from aggregated smart charging electric vehicles," *CIREN-Open Access J.*, vol. 2017, no. 1, pp. 1664–1668, Oct. 2017.
- [38] S. Izadkhast, P. Garcia-Gonzalez, and P. Frías, "An aggregate model of plug-in electric vehicles for primary frequency control," *IEEE Trans. Power Syst.*, vol. 30, no. 3, pp. 1475–1482, May 2015.
- [39] R. Hermans, M. Almassalkhi, and I. Hiskens, "Incentive-based coordinated charging control of plug-in electric vehicles at the distribution-transformer level," in *Proc. Amer. Control Conf. (ACC)*, Jun. 2012, pp. 264–269.
- [40] *Curve Ahead: The Future of Commercial Fleet Electrification*, GreenBiz, United Parcel Service Amer., Atlanta, GA, USA, Oct. 2018.
- [41] R. Carli and M. Dotoli, "A distributed control algorithm for optimal charging of electric vehicle fleets with congestion management," *IFAC-PapersOnLine*, vol. 51, no. 9, pp. 373–378, 2018.
- [42] M. R. Almassalkhi and I. A. Hiskens, "Model-predictive cascade mitigation in electric power systems with storage and renewables—Part I: Theory and implementation," *IEEE Trans. Power Syst.*, vol. 30, no. 1, pp. 67–77, Jan. 2015, doi: [10.1109/TPWRS.2014.2320982](https://doi.org/10.1109/TPWRS.2014.2320982).
- [43] A. Engelmann, Y. Jiang, T. Muhlfordt, B. Houska, and T. Faulwasser, "Toward distributed OPF using ALADIN," *IEEE Trans. Power Syst.*, vol. 34, no. 1, pp. 584–594, Jan. 2019.
- [44] A. Engelmann, Y. Jiang, B. Houska, and T. Faulwasser, "Decomposition of nonconvex optimization via bi-level distributed ALADIN," *IEEE Trans. Control Neww. Syst.*, vol. 7, no. 4, pp. 1848–1858, Dec. 2020.
- [45] S. Boyd, "Notes on decomposition methods," Stanford Univ., Stanford, CA, USA, Tech Rep. EE364B, Jan. 2007.
- [46] D. P. Bertsekas, *Convex Optimization Algorithms*. Belmont, MA, USA: Athena Scientific, 2015.
- [47] J. Wamburu, S. Lee, P. Shenoy, and D. Irwin, "Analyzing distribution transformers at city scale and the impact of EVs and storage," in *Proc. 9th Int. Conf. Future Energy Syst.*, New York, NY, USA, Jun. 2018, pp. 157–167.
- [48] F. Hourai, I. Huang, and M. A. A. Faruque, "Modeling and simulation of the EV charging in a residential distribution power grid," in *Proc. IEEE Green Energy Syst. Conf.*, Nov. 2013, pp. 1–5.
- [49] H. Nordman, N. Rafsback, and D. Susa, "Temperature responses to step changes in the load current of power transformers," *IEEE Trans. Power Del.*, vol. 18, no. 4, pp. 1110–1117, Oct. 2003.
- [50] M. T. Isha and Z. Wang, "Transformer hotspot temperature calculation using IEEE loading guide," in *Proc. Int. Conf. Condition Monitor. Diagnosis*, Apr. 2008, pp. 1017–1020.
- [51] *Permissible Loading Oil-Immersed Transformers Regulators*, U.S. Dept. Interior, Bureau Reclamation, Washington, DC, USA, 1991. [Online]. Available: <https://books.google.com/books?id=3HGOYgEACAAJ>
- [52] E. Schmidt. (Mar. 2018). *EV Clustered Charging Can be Problematic for Electrical Utilities*. [Online]. Available: <https://www.fleetcarma.com/ev-clustered-charging-can-be-problematic-electrical-utilities/>
- [53] Tesla. *Powerwall Connector*. Accessed: Oct. 13, 2021. [Online]. Available: <https://www.tesla.com/support/home-charging-installation/wall-connector>

- [54] J. Sears, D. Roberts, and K. Glitman, "A comparison of electric vehicle level 1 and level 2 charging efficiency," in *Proc. IEEE Conf. Technol. Sustain.*, Jul. 2014, pp. 255–258.
- [55] Inside EVs. *Monthly Plug-In EV Sales Scorecard: Historical Charts*. Accessed: Oct. 13, 2021. [Online]. Available: <https://insideevs.com/monthly-plug-in-ev-sales-scorecard-historical-charts/>
- [56] N. Nazir and M. Almassalkhi, "Guaranteeing a physically realizable battery dispatch without charge-discharge complementarity constraints," *IEEE Trans. Smart Grid*, early access, Sep. 2, 2021, doi: 10.1109/TSG.2021.3109805.



**Micah Botkin-Levy** received the bachelor's and master's degrees in electrical engineering from The University of Vermont, Burlington, VT, USA, in 2015 and 2019, respectively.

His graduate research focus was at the intersection of energy, optimization, and control with applications to transportation electrification. During his graduate studies, he spent time in Germany (working on optimization algorithms at the Karlsruhe Institute of Technology, Karlsruhe, Germany) and California

(working on energy storage valuation at the Electric Power Research Institute (EPRI), Palo Alto, CA, USA). He is currently a Senior Data Scientist at NextEra Energy Resources, where he works on helping fleets electrify their vehicles. His contributions include the development of data-driven decision platforms for evaluating the feasibility of vehicle electrification and leading the development of an operations product to co-optimize the charging of electric vehicles with distributed energy resources.



**Alexander Engelmann** (Member, IEEE) received the M.Sc. degree in electrical engineering and information technology and the Ph.D. degree in informatics from the Karlsruhe Institute of Technology, Karlsruhe, Germany, in 2016 and 2020, respectively.

Since 2020, he has been a Post-Doctoral Researcher with the Institute of Energy Systems, Energy Efficiency and Energy Economics, TU Dortmund University, Dortmund, Germany. His research focuses on distributed optimization and optimal control for power and energy systems.



**Tillmann Mühlpfordt** (Member, IEEE) received the Ph.D. degree from the Karlsruhe Institute of Technology, Karlsruhe, Germany, in 2019. He studied engineering cybernetics at Otto-von-Guericke University Magdeburg, Magdeburg, Germany.

He has spent research stays at the University of Melbourne, Melbourne, VIC, Australia, the Massachusetts Institute of Technology (MIT), Cambridge, MA, USA, the Ecole Polytechnique Fédérale de Lausanne (EPFL), Lausanne, Switzerland, and the Los Alamos National Laboratory (LANL),

Los Alamos, NM, USA. Since 2021, he has been working as a (Meta-)data Scientist at DB Systel GmbH, Frankfurt, Germany. His research interests include applied mathematics, numerical optimization, and uncertainty quantification.



**Timm Faulwasser** (Member, IEEE) received the Ph.D. degree from the Department of Electrical Engineering and Information Technology, Otto-von-Guericke University Magdeburg, Magdeburg, Germany, in 2021. He has studied engineering cybernetics at the University of Stuttgart, Stuttgart, Germany.

From 2008 until 2012, he was a member of the International Max Planck Research School for Analysis, Design and Optimization in Chemical and Biochemical Process Engineering, Magdeburg,

Germany. After his post-doctoral position at the École Polytechnique Fédérale de Lausanne, Lausanne, Switzerland, and the Karlsruhe Institute of Technology, Karlsruhe, Germany, he joined the Department of Electrical Engineering and Information Technology, TU Dortmund University, Dortmund, Germany, in 2019. His research interests are optimization and control of uncertain nonlinear systems and cyber-physical networks with applications in energy, mechatronics, process control, climate economics, and beyond.

Dr. Faulwasser serves as an Associate Editor for IEEE TRANSACTIONS ON AUTOMATIC CONTROL, IEEE CONTROL SYSTEMS LETTERS, *European Journal of Control*, and *Mathematics of Control, Systems, and Signals*.



**Mads R. Almassalkhi** (Senior Member, IEEE) received the B.S. dual degree in electrical engineering and applied mathematics from the University of Cincinnati, Cincinnati, OH, USA, in 2008, and the M.S.E. and Ph.D. degrees in electrical engineering: systems from the University of Michigan, Ann Arbor, MI, USA, in 2010 and 2013, respectively.

He is currently an Associate Professor with the Department of Electrical and Biomedical Engineering, The University of Vermont, Burlington, VT, USA, the Co-Founder of Packetized Energy, Burlington, and the Chief Scientist at the Pacific Northwest National Laboratory, Richland, WA, USA. Prior to joining The University of Vermont, he was a Lead Systems Engineer at energy startup company Root3 Technologies, Chicago, IL, USA. His research interests lie at the intersection of power systems, mathematical optimization, and control systems and focus on developing scalable algorithms that improve responsiveness and resilience of energy and power systems.

Dr. Almassalkhi is also serving as the Chair for the IEEE Power and Energy Society's Smart Buildings, Loads, and Customer Systems (SBLC) Technical Subcommittee on Loads.